Effects of tidal mixing at the Kuril Straits on North Pacific ventilation: Adjustment of the intermediate layer revealed from numerical experiments

Tomohiro Nakamura,[1,2] Takahiro Toyoda,[1,3] Yoichi Ishikawa,[4] and Toshiyuki Awaji[1,5]

Received 4 July 2005; revised 30 November 2005; accepted 27 December 2005; published 8 April 2006.

[1] The effects of tidal mixing at the Kuril Straits on the North Pacific intermediate layer are investigated using an ocean general circulation model. A comparison of numerical experiments with and without a tidal mixing effect suggests that tidal mixing at the Kuril Straits enhances the ventilation of the North Pacific intermediate layer. The enhanced ventilation results in both freshening and cooling down to $\sim$27.6 σ_θ. In particular, the simulated North Pacific Intermediate Water (NPIW) becomes fresher and denser (by 0.3 psu and 0.1 σ_θ at the maximum) and hence more realistic. The enhanced ventilation is caused both through the supply of the ventilated water from the Kuril Straits, which subsequently spreads along the subarctic and subtropical gyres, and through a modification of the circulation there. The ventilation of the supplied water in turn originates from a combination of tidally enhanced convection in the Okhotsk Sea and downward diffusion at the Kuril Straits as discussed in a previous paper. The former affects the upper part of the NPIW, while the latter is dominant in the denser layers. The circulation is modified through a dynamical adjustment to the mass input into an intermediate layer that is produced by the convergence of diapycnal transport due to the tidally enhanced convection and diffusion. The dynamical adjustment is conducted mainly through Kelvin waves which have the ability to induce intergyre flow along the western boundary and also by eastward moving long Rossby waves. The latter can be present under the influence of the wind-driven gyres for the second and higher baroclinic modes and act to spread information into the interior directly from the western boundary. As a direct consequence of this adjustment, transport of the ventilated water from the Kuril Straits to the subtropical gyre is enhanced by the intergyre flow along the western boundary, which appears as the southward intrusion of the Oyashio Current. The transported water leaves the coast to encircle the interior, and returns to the western boundary, eventually flowing into the equatorial region. Such equatorward transport associated with mass convergence in the intermediate layer is compensated by transport toward the Kuril Straits in the shallower and deeper layers, thereby enhancing both shallow and deep meridional overturning cells by 2–3 Sv. The above dynamical adjustment is thus central to our understanding of the ventilation of the intermediate layer and provides a basis for the analytical model developed in an accompanying paper.

Citation: Nakamura, T., T. Toyoda, Y. Ishikawa, and T. Awaji (2006), Effects of tidal mixing at the Kuril Straits on North Pacific ventilation: Adjustment of the intermediate layer revealed from numerical experiments, *J. Geophys. Res.*, *111*, C04003, doi:10.1029/2005JC003142.

1. Introduction

[2] The ventilation originating in and around the subarctic Pacific Ocean carries fresh, subarctic surface water into the intermediate layer from the subarctic to the subtropical North Pacific. One prominent indication of this ventilation/freshening is the North Pacific Intermediate Water (NPIW), which is characterized by a well defined salinity minimum around 26.8 σ_θ [e.g., *Sverdrup et al.*, 1942]. The NPIW spreads over most of the subtropical gyre, and intrudes even into the tropics [e.g., *Talley*, 1993]. Since the above ventilation process involves the storage of large amounts

[1]Frontier Research Center for Global Change, JAMSTEC, Yokohama, Japan.
[2]Now at Institute of Low Temperature Science, Hokkaido University, Sapporo, Japan.
[3]Formerly at Department of Geophysics, Graduate School of Science, Kyoto University, Kyoto, Japan.
[4]Department of Geophysics, Graduate School of Science, Kyoto University, Kyoto, Japan.
[5]Also at Department of Geophysics, Graduate School of Science, Kyoto University, Kyoto, Japan.

0148-0227/06/2005JC003142$09.00

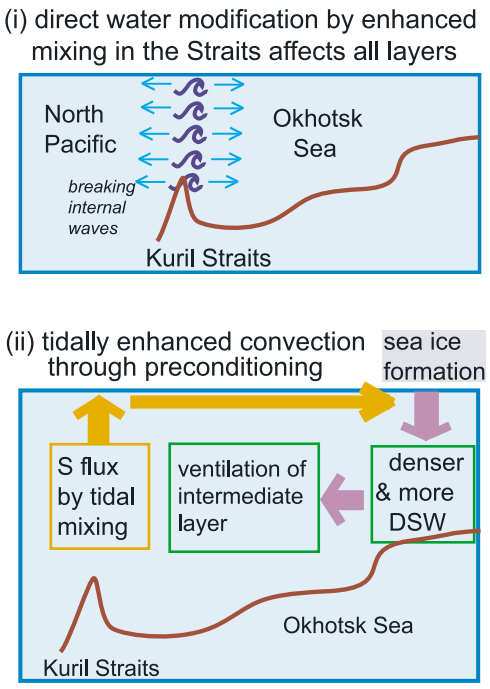

Figure 1. Schematic view of the two roles of tidal mixing in the Kuril Straits in ventilation of the Okhotsk Sea.

of heat, fresh water, and greenhouse gases such as CO_2 in the ocean [e.g., *Yamanaka and Tajika*, 1996], clarification of the intermediate water ventilation process is important in understanding, modeling, and predicting the potential response of the North Pacific intermediate layer to long-term variability.

[3] The main source of low-salinity water in the NPIW is considered to be the Okhotsk Sea [e.g., *Talley*, 1991; *Yasuda et al.*, 1996], although the low salinity sources at the top of the NPIW (say, 26.7–26.8 σ_θ) are also thought to lie in the Alaskan Gyre [e.g., *Van Scoy et al.*, 1991; *You et al.*, 2000] and in the subarctic, winter mixed layer [*Talley*, 1993; *Talley et al.*, 1995; *Talley and Yun*, 2001]. In the Okhotsk Sea, convection associated with sea ice formation in winter produces Dense Shelf Water (DSW), whose maximum density reaches ~27.0 σ_θ [*Kitani*, 1973; *Alfultis and Martin*, 1987; *Martin et al.*, 1998; *Gladyshev et al.*, 2000]. The DSW transforms Okhotsk Sea intermediate water, which subsequently enters the Pacific, thereby modifying the subarctic Pacific water [e.g., *Yasuda*, 1997; *Kono and Kawasaki*, 1997a; *Watanabe and Wakatsuchi*, 1998]. While the main part of the modified subarctic water remains in the subarctic gyre, a portion intrudes into the subtropical gyre mainly near the western boundary, leading to the formation of new NPIW [e.g., *Yasuda et al.*, 1996].

[4] While this DSW is the densest water subducted in and around the North Pacific [*Talley*, 1991], the ventilation occurring in the North Pacific reaches much denser layers (27.4 ~ 27.6 σ_θ) as indicated by Chlorofluorocarbons (CFCs) observations [*Watanabe et al.*, 1994; *Warner et al.*, 1996; *Fine et al.*, 2001] (convection in the Japan Sea is not considered here since this sea is separated by very shallow straits). What processes ventilate the lower part (say, 27.0 ~ 27.6 σ_θ) of the North Pacific intermediate layer?

[5] The cabbeling effect is also unlikely because the density increase it causes during mixing of subarctic and subtropical waters is less than 0.02 σ_θ below the 27.0 σ_θ density layer [*Talley and Yun*, 2001]. In addition, the necessary conditions for double diffusion are not met below the density layer of ~26.8 σ_θ in the North Pacific or 26.8 ~ 27.2 σ_θ in the Okhotsk Sea (where the NPIW salinity minimum in the subtropics or the temperature maximum layer in the subarctic is present), and hence mechanical mixing is more likely. This expectation is consistent with the observed nutrients distributions which suggest the occurrence of enhanced vertical mixing somewhere in the North Pacific so that nutrient rich water of the deep ocean is brought up into the intermediate layer [*Sarmiento et al.*, 2004].

[6] Among mechanical mixing mechanisms, one likely candidate is vertical mixing at the Kuril Straits [e.g., *Talley*, 1991], that is induced by tides [e.g., *Nakamura et al.*, 2000a]. The Kuril Straits are located between the North Pacific and the Okhotsk Sea. The ventilated water in the lower intermediate layer also originates around the Okhotsk Sea, according to the observed distributions of CFCs [*Warner et al.*, 1996] and numerical simulations [*Yamanaka et al.*, 1998a, 1998b]. In particular, the Kuril Straits have the lowest salinity and highest oxygen on the deep density layers (27.0 ~ 27.6 σ_θ), indicating that ventilation reaching these deep layers occurs locally in the Kuril Straits [e.g., *Yasuoka*, 1968; *Kitani*, 1973; *Kawasaki and Kono*, 1994; *Freeland et al.*, 1998; *Aramaki et al.*, 2001]. This is probably due to downward diffusion by locally enhanced vertical mixing, since the outcropping of such dense isopycnal surfaces ($\gtrsim$27.1 σ_θ) have never been observed in either the Okhotsk Sea or the open North Pacific (including the Bering Sea) [e.g., *Kitani*, 1973; *Talley*, 1991].

[7] The enhanced vertical mixing is in fact made possible by the subinertial, diurnal tides [*Nakamura et al.*, 2000a, 2000b; *Nakamura and Awaji*, 2001, 2004]. This is because the tidal flow is considerably intensified around the Kuril Straits (~2 m s^{-1}) due to the effective amplification of topographically trapped waves generated by the subinertial diurnal tides, in addition to the effect of topographic contraction, so that internal lee waves of large amplitudes (~100 m) are thought to be generated over topographic features and break, eventually leading to the enhanced vertical mixing. The mixing occurs from the surface to the sill bottom and all along the Kuril Island Chain, and is particularly intense over shallow sills or banks where the maximum diffusivity may exceed 1000 cm^2 s^{-1}.

[8] However, although the above studies suggest the importance of tidally induced vertical mixing (hereafter, tidal mixing) at the Kuril Straits, its effect is still not well understood. For example, the recent results of numerical experiments performed by *Nakamura et al.* [2006] have suggested that tidal mixing at the Kuril Straits is fundamental for the formation of the fresh and cold Okhotsk Sea water even at the NPIW salinity minimum density layer. According to their study, tidal mixing exerts its influence through two processes, as shown schematically in Figure 1. First, tidal mixing directly modifies water properties in the Kuril Straits. This modification process

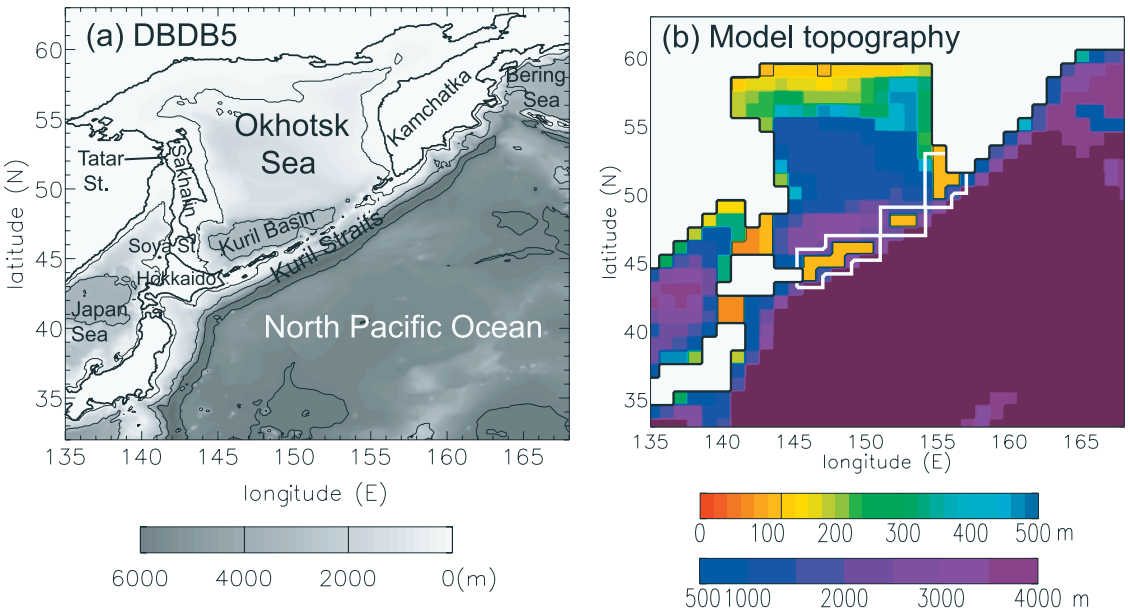

Figure 2. (a) Bottom topography around the Okhotsk Sea. Contours are drawn at 200, 3000, and 6000 m depth. (b) Model topography around the Okhotsk Sea. Thick white lines indicate the region of enhanced vertical diffusion in the Tmix case, while thick black lines indicate land boundaries.

involves downward diffusion, which enhances the ventilation and freshening of the intermediate and deeper layers (the freshening occurs because salinity generally increases with depth in the subarctic Pacific and the Okhotsk Sea). Second, tidal mixing in the Kuril Straits preconditions the DSW production in the northern Okhotsk Sea, as follows. Tidal mixing makes water in the upper layer saltier because of the salinity stratification. This saltier water is carried northward to the DSW production region by the wind-driven basin-scale cyclonic circulation in the Okhotsk Sea. Accordingly, the DSW produced in a mixed environment is relatively saltier and hence denser and there is an increase in production rate, when DSW is defined by density and potential temperature in the traditional fashion. We call this second process "tidally enhanced convection". The tidally enhanced convection strengthens the ventilation and freshening of the intermediate layer (the latter occurs since DSW is so cold that it is less saline when compared on an isopycnal surface). The above results imply that the Okhotsk Sea water that is freshened and ventilated through the above two processes flows into and spreads over the North Pacific. In parallel with this, tidal mixing at the Kuril Straits also affects density layers around the NPIW salinity minimum layer as well as the lower intermediate layer. The tidal mixing should thus have a greater impact on the North Pacific than previously thought.

[9] From a dynamical point of view, both the diffusion and enhanced convection induced by tidal mixing will change potential vorticity (PV) supplied to the North Pacific. Such a change in PV is expected to travel eastward roughly along the Sverdrup flow lines and thereby affect the circulation en route, on the basis of the ventilated thermocline theory [e.g., *Pedlosky*, 1996]. The investigation of such dynamical adjustments and associated changes in circulation will benefit our understanding of the North Pacific intermediate layer circulation. In addition, two important factors need to be considered. First, the PV input is given from the west (of the subpolar gyre), instead of the east or the interior (of the subtropical gyre), where responses have been extensively investigated [e.g., *Luyten and Stommel*, 1986; *Liu*, 1993; 1999; *Sirven and Frankignoul*, 2000; *Stephens et al.*, 2001; *Dewar and Huang*, 2001; *Samelson*, 1998]. Secondly, the convection in the Okhotsk Sea does not reach great depths in contrast to the deep convection in the North Atlantic, where the response can be understood on the basis of the work of *Kawase* [1987]. Thus an investigation of the adjustment mechanism is of theoretical interest.

[10] In this study, we therefore investigate the effects of tidally enhanced vertical mixing at the Kuril Straits on the ventilation of the North Pacific intermediate layer. To this end, numerical experiments with and without tidally enhanced vertical mixing at the Kuril Straits are conducted, using an ocean general circulation model (OGCM). On the basis of the results obtained here, an analytical model of the intermediate layer ventilated from the west is developed in an accompanying paper (T. Nakamura et al., manuscript in preparation, 2006) (hereafter Part 2).

[11] The rest of the paper is organized as follows. The numerical model and experimental design are described in section 2. By comparing the cases with and without a tidal mixing effect, the effects on water mass structures are examined in section 3, where we focus on the differences in salinity and PV distributions in the intermediate layer and on the temperature profile of the mesothermal water in the western subarctic. Dynamical adjustments due to tidal mixing at the Kuril Straits in the intermediate layer are analyzed in section 4, and the resulting differences in the intermediate layer circulation and meridional overturning are shown in section 5. The sensitivity of the results to tidal-

Table 1. List of Experiments

case	increase in K_z at the Kuril Straits
Main Experiments	
Ctrl	none
Tmix (Kz200)	200 cm^2s^{-1}
Sensitivity Experiments	
Kz10	10 cm^2s^{-1}
Kz20	20 cm^2s^{-1}
Kz30	30 cm^2s^{-1}
Kz50	50 cm^2s^{-1}
Kz100	100 cm^2s^{-1}
Kz200 (Tmix)	200 cm^2s^{-1}
Kz300	300 cm^2s^{-1}
Kz500	500 cm^2s^{-1}
Kz1000	1000 cm^2s^{-1}
noDD	200 cm^2s^{-1}

Vertical diffusivity coefficient, K_z, is increased over the sills in the Kuril Straits except for the Ctrl case. In the noDD case, double-diffusion parameterization is excluded.

mixing strength is discussed in section 6, and a summary and discussion is presented in section 7.

2. Model and Experimental Design

[12] The model and experimental design are the same as those of *Nakamura et al.* [2006] and are summarized in the following. The model used is an OGCM developed at Kyoto University [*Toyoda et al.*, 2004; *Nakamura et al.*, 2006], which solves the primitive equations in spherical coordinates. For a realistic reproduction of the subduction process, this model adopts a third-order advection scheme for the tracer equation (UTOPIA and QUICKEST [*Hasumi and Suginohara*, 1999]), in addition to isopycnal diffusion with eddy parameterization [*Redi*, 1982; *Gent and McWilliams*, 1990] (hereafter GM90) and a turbulence closure mixed layer scheme [*Noh and Kim*, 1999]. In the latter schemes, both the isopycnal and GM90 diffusivity coefficients are set to 10^7 cm^2 s^{-1}, and the background vertical and diapycnal diffusivity and viscosity coefficients are set to 0.01 cm^2 s^{-1}. To accurately simulate the convection associated with sea ice formation in the Okhotsk Sea, a sea ice model is incorporated on the basis of the works of *Ikeda* [1989a, 1989b] and *Ikeda et al.* [1988]. This model is a *Hibler* [1979] two-category ice model and includes both dynamic and thermodynamic processes (the simulated ice production and distribution in the Okhotsk Sea are basically similar to those observed [*Nakamura et al.*, 2006]). The effect of double diffusion is also included [*Merryfield et al.*, 1999; *Schmitt*, 1981; *Fedorov*, 1988], since it is considered to affect the top of the NPIW [*Talley and Yun*, 2001], although it turns out to be insignificant in the deeper layers. For the momentum equation, an enstrophy conserving scheme (in addition to momentum and kinetic energy) is incorporated [*Ishizaki and Motoi*, 1999] to yield an accurate simulation of the expected circulation change. The partial cell method is used for a better representation of bottom topography.

[13] The model domain is virtually global (75°S–75°N) with a horizontal resolution of 1° × 1°. In the vertical, the 34 levels used are spaced from 20m at the sea surface to 400m in the abyss. The model topography is based on a horizontal average of DBDB5 (U.S. National Geophysical Data Center), whose original resolution is 1/12° × °1/12. However, the averaged depths along the Kuril Island Chain then become around 2000 m, much deeper than the observations. Actually, sills in the Kuril Straits are shallow (≲200 m), except for two main deep straits, so that the Kuril Island Chain effectively blocks the western boundary current of the subarctic Pacific from entering the Okhotsk Sea. Thus we have decreased depths in the Kuril Straits from the averaged values, except for the two main straits (Figure 2). This modification enables us to reproduce the basic features of the western boundary current and the circulation in the Okhotsk Sea.

[14] The initial values of potential temperature and salinity are taken from the World Ocean Atlas 1994 Monthly Data compilation (WOA94 [*Levitus and Boyer*, 1994; *Levitus et al.*, 1994]). Sea surface fluxes are calculated with the bulk formulae [*Röske*, 2001; *Ikeda*, 1989b; *da Silva et al.*, 1994]. The atmospheric and river runoff data used are based on the climatological monthly mean data compiled by *Röske* [2001], which is in turn based on the European Centre for Medium-Range Forecasts (ECMWF) reanalysis data. The ice and oceanic data used in calculating the surface fluxes are taken from simulated values, as is often the case in ice-ocean coupled models. Note that the heat and fresh water fluxes calculated with the bulk formulae are adjusted using the flux correction method (i.e., a weak relaxation term is added) with a relaxation timescale of 60 days, as recommended by, for example, *Barnier et al.* [1995] and *Weaver and Hughes* [1996]. This is because although the ECMWF reanalysis data is considered as one of the most realistic data sets, it still has uncertainty due to both sparse observations over the ocean and the incompatibility between atmosphere and ocean models, and thus the simultaneous use of both bulk formulae and adequate relaxation has been recommended. Nevertheless, the fluxes due to bulk formulae is dominant in our model. In fact, the comparison with similar experiments but with a relaxation time of 30 days does not show a qualitative difference, as will be shown in section 7.

[15] In addition, restoration of potential temperature and salinity to those of WOA94 is applied at the northern and southern boundaries, at the exits of the Mediterranean and Red Seas, and in layers deeper than 2000 m with the same timescale as that of the flux correction. The restoration in the deep layers reduces the spinup time by circumventing the spinup of the abyssal circulation.

[16] Two main experiments were conducted (Table 1), after a 40-year spinup by which time the model ocean had reached a state of approximate equilibrium. The first of these was a control experiment obtained by a further 40-year integration (hereafter the "Ctrl" case). The second was an experiment for the case with a tidal mixing effect (the "Tmix" case). This case was obtained by a 40-year integration after the spinup, but with the vertical diffusivity coefficient over the sills at the Kuril Straits increased by 200 cm^2 s^{-1} (Figure 2), on the basis of the results of *Nakamura et al.* [2000b] and *Nakamura and Awaji* [2004]. In this Tmix case, the flux correction was not applied around the Kuril Straits in order to avoid artificial heat and fresh water fluxes which would arise owing to the fact that the WOA94 data does not resolve the vertically mixed water in the Kuril Straits.

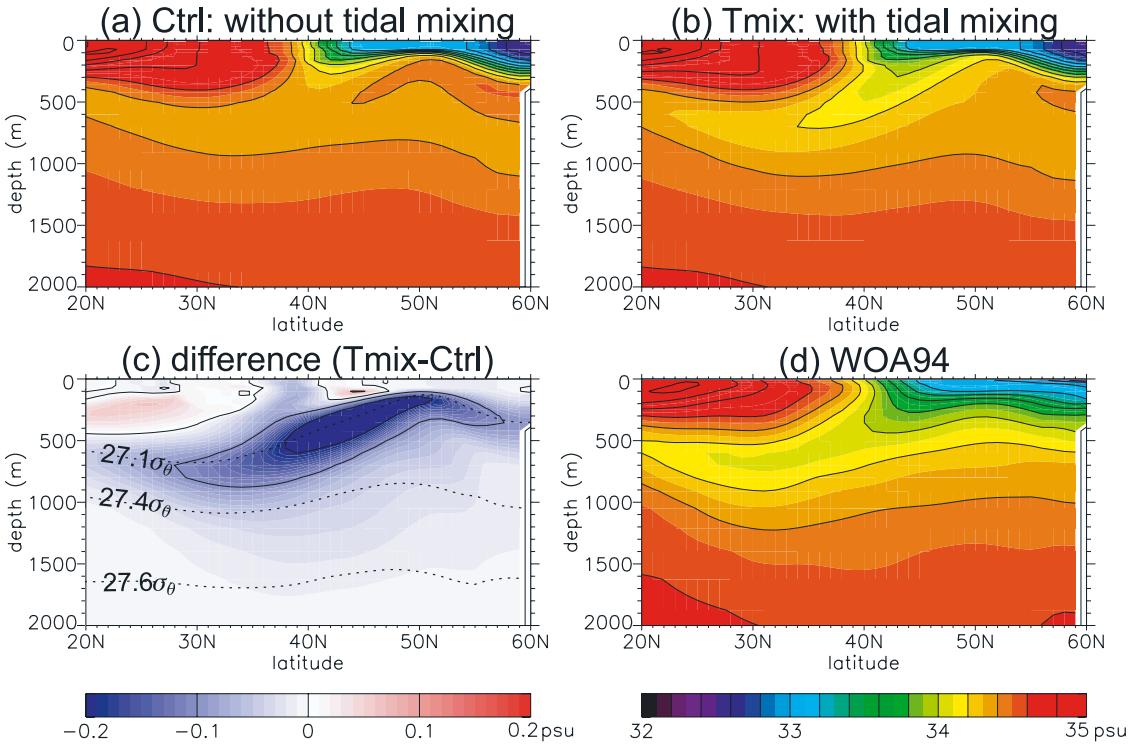

Figure 3. Meridional section of salinity at 165°E in the (a) Ctrl and (b) Tmix cases. (c) The difference between the Ctrl and Tmix cases (Tmix-Ctrl). Dotted lines in Figure 3c indicate 27.1, 27.4, and 27.6 σ_θ isopycnal surfaces, respectively. (d) Salinity from WOA94.

[17] The final year of the integration (i.e., the 80th year) is used in the analysis below, except for the investigation of the temporal evolution after the addition of tidal mixing in section 4.1. The adjustment to tidal mixing is largely finished in the North Pacific after 40 years, although the adjustment of the temperature and salinity fields in other basins associated with the change in the global thermohaline circulation has not yet finished. In fact, the results of a 30-year integration after the addition of tidal mixing and those of a 40-year integration are similar to each other (not shown).

[18] It should be noted that tides were not directly simulated and that their effect was parameterized through local increase in vertical diffusion. This parameterization does not consider the total effect of a tidal process (or tidal mixing), even though vertical diffusion is a major effect at the spatial scale under consideration [e.g., *Schiller et al.*, 1998; *Hibiya et al.*, 1998]. The value of vertical diffusion is increased at all depths in the Kuril Straits as a first approximation. The specified value (200 $cm^2\ s^{-1}$) roughly corresponds to twice that induced by the K_1 tide alone [*Nakamura and Awaji*, 2004]. The reason for this selection is that the total tidal flow speed in the Kuril Straits is roughly twice as large as that of the K_1 component alone, according to the tidal simulations reported by *Nakamura et al.* [2000a]. Also, the use of this value resulted in a reasonable reproduction of water transformation in the Okhotsk Sea [*Nakamura et al.*, 2006]. Taking these facts into account, the above rough estimate of diapycnal diffusivity was used for a basic investigation of the impacts of tidal mixing on the North Pacific.

[19] In order to examine the sensitivity of the ventilation of the North Pacific intermediate layer to the strength of the tidal mixing, eight additional experiments were conducted, in which the vertical diffusivity coefficient was varied from 10 to 1000 $cm^2\ s^{-1}$ (Kz10 to Kz1000 cases, respectively; Table 1). The results of these further experiments are discussed in section 6.

3. Differences in Water Mass Structures

[20] To see how tidal mixing at the Kuril Straits affects ventilation of the intermediate layer in the North Pacific, we first compare the salinity distributions of the Ctrl and Tmix cases. This is because freshening in these regions indicates an influence from the surface water of the subarctic Pacific and/or its marginal seas since a freshening influx can only come from this layer. The associated changes in temperature and PV are also examined.

3.1. Salinity Distribution in a Meridional Section

[21] Salinity distributions derived from the Ctrl and Tmix cases and from the WOA94 data set at 165°E from the subarctic to subtropical gyres are shown in Figure 3. Comparison of the two simulations shows that tidal mixing at the Kuril Straits causes a significant freshening of the intermediate water, as freshened water is supplied from the Kuril Straits and subsequently spreads out. This indicates that the addition of tidal mixing there leads to a strengthening and deepening of the ventilation in the North Pacific.

[22] On closer examination, the freshening consists of two features. First, the salinity minimum layer extending

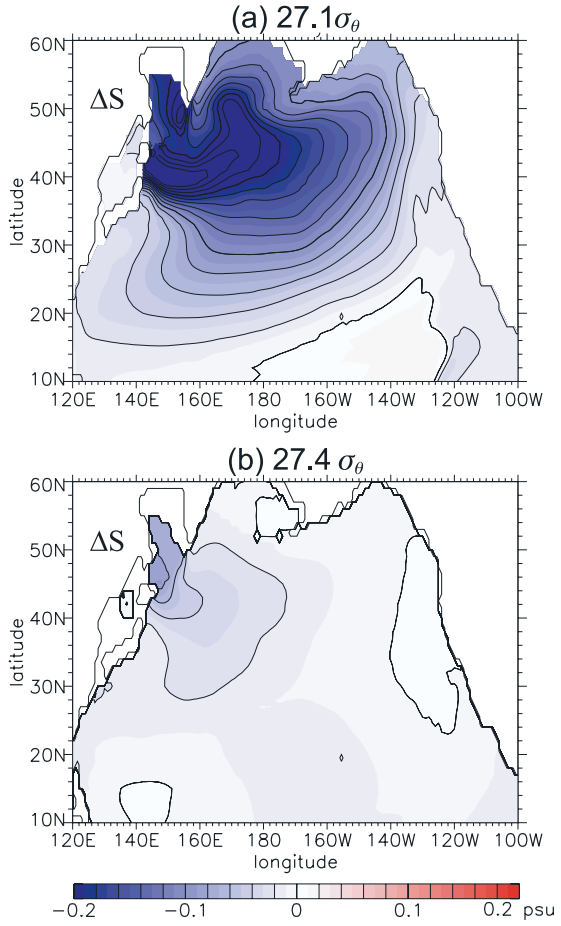

Figure 4. Maps of salinity difference between the Ctrl and Tmix cases on (a) 27.1 σ_θ and (b) 27.4 σ_θ isopycnal surfaces.

from the subarctic to subtropics, which is the feature of the NPIW, is effectively freshened and deepened. As a result, salinity there decreases by up to 0.3 psu and its density increases by about 0.1 σ_θ (Figure 3c), leading to a better reproduction of the NPIW. Secondly, the deeper layers are also significantly freshened. This deep freshening is still appreciable around 1500 m depth or the 27.6 σ_θ density layer (Figure 3c). The occurrence of freshening or ventilation in the North Pacific down to such deep layers is consistent with the CFCs observations [e.g., *Warner et al.*, 1996].

[23] Such difference in freshening intensity between the shallower and deeper layers is associated with the two freshening processes in the Okhotsk Sea described in the introduction. The shallower, well-freshened water component concentrates on the 27.1 σ_θ surface (Figure 3c), suggesting that it mainly originates from the tidally enhanced convection in the Okhotsk Sea. In fact, its density roughly corresponds to the DSW density (although density increases somewhat owing to effects of tidal mixing and cabbeling). This DSW is produced through the tidally enhanced convection in the Okhotsk Sea in the Tmix case but is almost absent in the Ctrl case [*Nakamura et al.*, 2006]. In contrast, the deep freshening extends far beyond the layer with the DSW density, implying that it is caused mainly by the tidally induced diapycnal mixing at the Kuril Straits.

[24] On the basis of the above difference in the driving mechanism of downward conduction of a freshening flux, we tentatively categorize the North Pacific intermediate layer into upper and lower parts. The upper part is reached by ventilation due to both convection in the northern part of the Okhotsk Sea and tidal mixing at the Kuril Straits, and corresponds to the top and salinity-minimum layers of the NPIW. The lower part is ventilated almost solely by tidal mixing at the Kuril Straits. This categorization is convenient in discussing the effects of tidal mixing at the Kuril Straits.

3.2. Horizontal Distributions

[25] Figure 4 shows the horizontal spreading of salinity difference between the Ctrl and Tmix cases on the 27.1 and 27.4 σ_θ isopycnal surfaces: The former corresponds to the intensely freshened, upper intermediate layer and the latter to the lower intermediate layer. On both surfaces, the largest decrease in salinity occurs around the Kuril Straits. This fact confirms that the origin of the freshening discussed above is located here.

[26] On the upper intermediate layer, the freshening spreads to the entire subarctic region and to virtually the whole of the subtropics, and even extends to the equatorial region near the western boundary. This distribution is in broad agreement with the observed distribution of the NPIW [*Talley*, 1993], confirming that tidal mixing at the Kuril Straits has an important role in the formation of the NPIW.

[27] On the lower intermediate layer, a similar pattern of spreading is seen, but its area is reduced considerably. In particular, the freshened region in the subtropics shrinks toward the northwest corner of the gyre, as the area of the pool region reduces with increasing density. Such a reduction in the freshened area also occurs in the subarctic but is located toward the southwest corner of the gyre. These results suggest that the freshened water supplied from the Kuril Straits flows into the pool regions in both subarctic and subtropical gyres, consistent with a result of an analytical model described in Part 2.

3.3. Temperature in the Subarctic Intermediate Layer

[28] In contrast to the subtropics, the intermediate layer of the subarctic Pacific is characterized by a local maximum of potential temperature in the vertical direction, which is called the "mesothermal water" [e.g., *Uda*, 1963]. Figure 5 compares vertical profiles of potential temperature derived from the Ctrl and Tmix cases and from the WOA94 data set near the center of the western part of the subarctic gyre, where typical mesothermal water is found [*Ueno and Yasuda*, 2000].

[29] Potential temperature in the Tmix case decreases by up to 1°C relative to the Ctrl case. Such cooling leads to the reproduction of a more realistic profile of mesothermal water, particularly below the seasonal thermocline (say, below 150 m) and is associated with the freshening described in the previous section. In fact, since σ_θ depends solely on salinity and potential temperature, the salinity decrease on the isopycnal surfaces shown in Figure 4 implies a corresponding decrease in potential temperature.

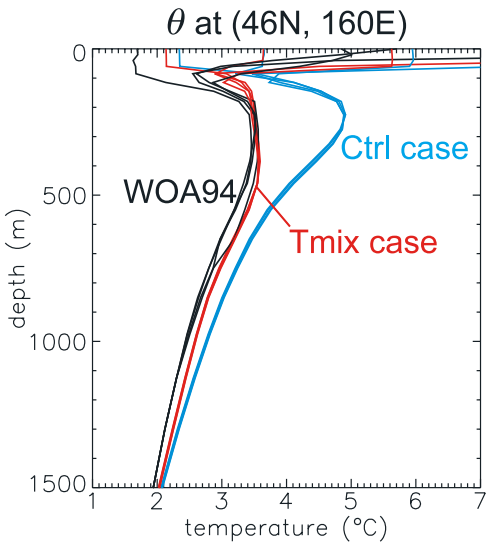

Figure 5. Vertical profiles of potential temperature at (46°N, 160°E), which roughly corresponds to the center of the western subarctic gyre. Blue, red, and black lines are those of the Ctrl and Tmix cases and WOA94, respectively. For each case, four lines are drawn to show those in all seasons.

In other words, the enhanced ventilation brings fresher and colder water into the intermediate density layer.

3.4. Potential Vorticity

[30] Associated with the above change in salinity and temperature, the PV field is also modified. Maps of PV difference on the upper and lower intermediate layers are shown in Figure 6 (~27.1 and 27.4 σ_θ isopycnal surfaces, respectively). On the upper intermediate layer, the lower PV water, that is produced through the tidally enhanced convection in the Tmix case, is supplied from the Okhotsk Sea to the southern part of the subarctic gyre and to the subtropical gyre. The PV increase in the northern part of the subarctic gyre is associated with the upward Ekman pumping, which works to reduce the depth of the density layer as it circulates in the gyre to the north. When tidal mixing is added at the Kuril Straits, the intermediate layer becomes thicker (i.e., lower PV). Associated with this, the upper part becomes shallower and progressively shallows during the circulation and thus it receives more of an influence from Ekman pumping and/or mixed layer.

[31] On the lower intermediate layer, PV values increase in the subarctic gyre and decrease in the subtropical gyre owing to the tidal mixing effect. In the former case, the PV increase is consistent with the view that the main cause of the ventilation of such deep layers is diapycnal mixing at the Kuril Straits, since convection is generally accompanied by low PV water. In fact, as will be shown in section 4.1, vertical mixing at the Kuril Straits generally produces a net mass flux to the shallower layers from the deeper layers in this experiment. As a result, the deeper layers become thinner through enhanced vertical mixing and hence PV increases. This change spreads over the subarctic gyre, resulting in the PV increase on this layer. On the other hand, the PV decrease in the subtropical gyre is due to an enhanced transport of subarctic, lower PV water to the subtropics. This will be described in the next sections.

[32] The changes taking place in PV distributions are usually accompanied by a modification of the circulation. Some PV changes themselves are induced by the change in circulation. This in turn implies that the change in water mass structure can be caused by variations in not only the properties of the source water supplied from the Kuril Straits but also the paths through which the modified source water is distributed. We will thus investigate the mechanism of the latter and the resulting change in circulation in the following sections. As for the change in source water properties, the reader is referred to *Nakamura et al.* [2006].

4. Thermohaline Adjustment in Intermediate Layers

[33] To facilitate a description of the change in circulation expected from the change in PV, we identify in advance the important dynamical elements responsible for the circulation change in this section. This is done by examining the initial adjustment process to the forcing arising from the addition of tidal mixing at the Kuril Straits.

4.1. Forcing From the Kuril Straits

[34] First, we examine the vertical structure of the forcing given to the North Pacific. Figure 7 compares the initial

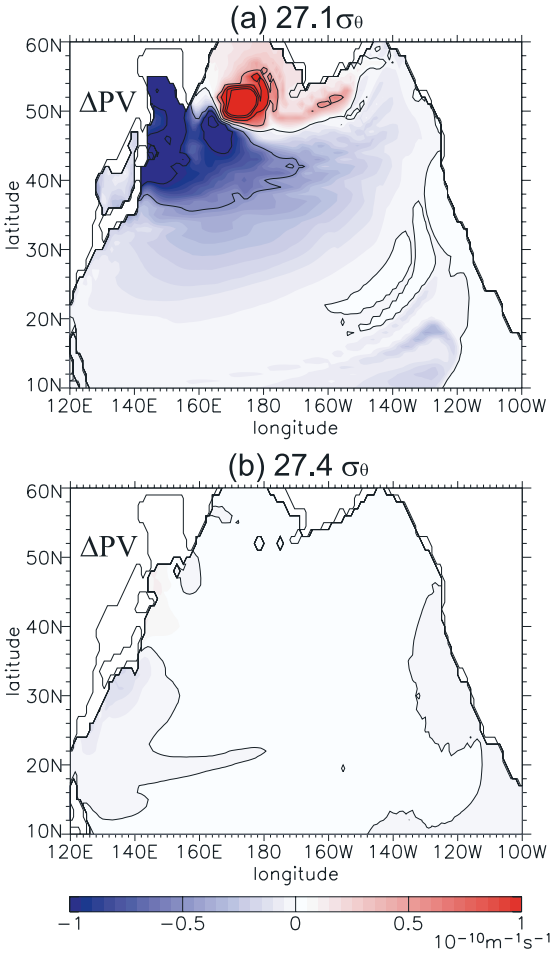

Figure 6. Same as Figure 4, but for potential vorticity.

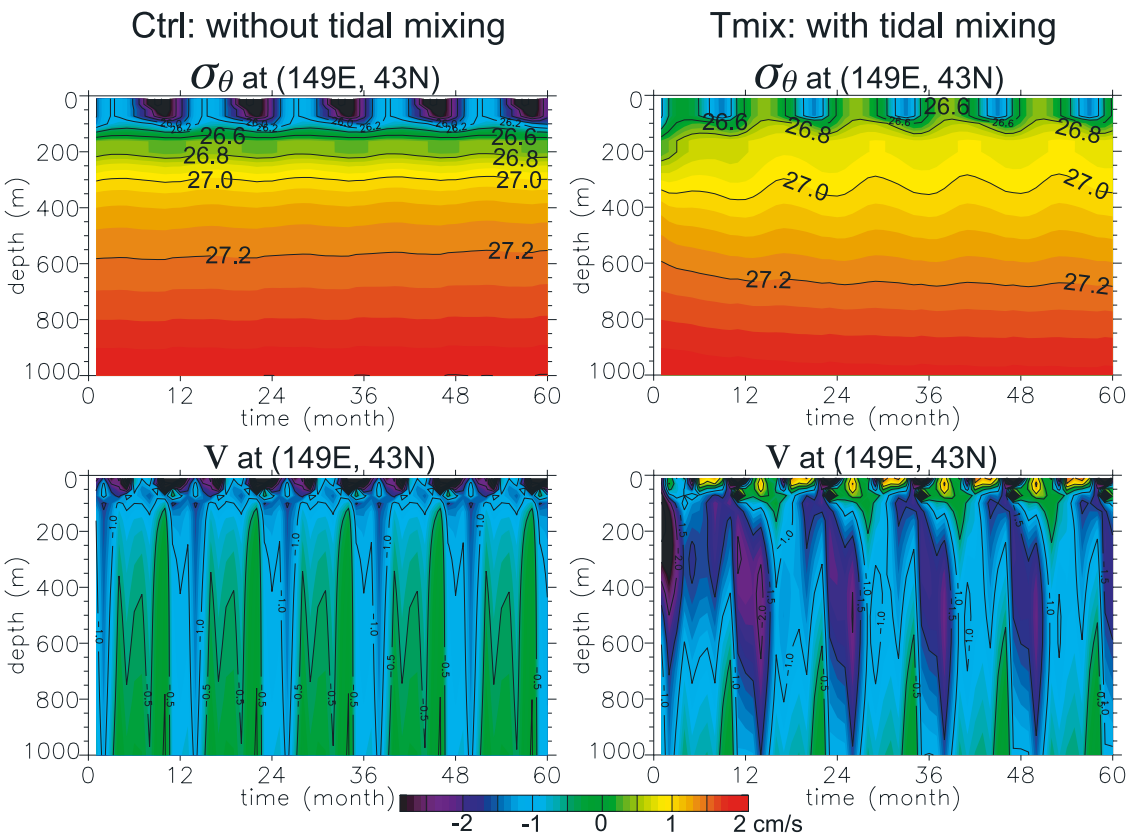

Figure 7. Initial evolution of vertical profiles of (top) density (σ_θ) and (bottom) meridional velocity at (149°E, 43°N), after addition of tidal mixing for the (left) Ctrl and (right) Tmix cases. The site is located at the main exit of the Kuril Straits on the North Pacific side. Month 1 is January and corresponds to the first month from the addition of tidal mixing. The contour interval is 0.2 σ_θ for density and is 0.5 cm s^{-1} for velocity.

evolution of vertical profiles of density (σ_θ) and meridional velocity in the Ctrl and Tmix cases on the Pacific side of the Bussol Strait (the main exit of the Okhotsk Sea water, located in the central part of the Kuril Straits) after the addition of tidal mixing (from the first day of the 41st model year).

[35] In the first few months, the intermediate density layer generally becomes deeper and thicker (i.e., PV is lowered) in the Tmix case. Because only vertical diffusion at the Straits can work at this stage, vertical diffusion is responsible for both the deepening and thickening. This continues until an equilibrium is reached.

[36] The deepening is caused by entrainment from the deeper layer due to vertical diffusion. Such entrainment results from the fact that around the Kuril Straits the vertical salinity distribution, which almost determines density stratification, shows a convex structure as a whole (i.e., $\partial^2\rho/\partial z^2 < 0$ [e.g., *Watanabe and Wakatsuchi*, 1998]), so that a down-gradient type vertical diffusion decreases salinity and thus density. This density decrease causes a deepening of the isopycnal surfaces and thus can be interpreted as "diapycnal mass transport" from the denser layers to the lighter layers. On the other hand, the thickening is caused by entrainment from the shallower layers as well as the deeper layers. The former occurs since the value of the gradient, $\partial\rho/\partial z$ is roughly zero near the sea surface and hence the inequality $\partial^2\rho/\partial z^2 > 0$ holds around there. Accordingly, density increases and isopycnal surfaces shallow near the sea surface, so that diapycnal transport is induced from the lighter, shallower layers.

[37] After the second winter, further thickening occurs in the upper intermediate layer (around month 18), as the influence of the enhanced convection taking place in the inner part of the Okhotsk Sea reaches the Kuril Straits. In fact, as an implication of the seasonality inherent in a convection process, this further thickening of the upper intermediate layer is accompanied by a strong seasonal variation with a maximum thickness occurring in spring, which is absent in the Ctrl case.

[38] Overall, the addition of tidal mixing makes the intermediate layer deeper and thicker, which in turn will induce baroclinic responses. The deepening is associated with downward movement of isopycnal surfaces with the peak at the intermediate layer. Accordingly, the first baroclinic mode response is mainly excited together with the higher mode responses depending on the vertical distribution of the net diapycnal transport. In contrast, in association with the thickening centered around 27.1 σ_θ, the isopycnal surfaces of the upper part of the intermediate layer move upward while those of the lower part move downward. Such a vertical movement in the opposite direction excites the second and/or higher baroclinic mode response. This is similar to the case of subduction enhanced by cooling in a

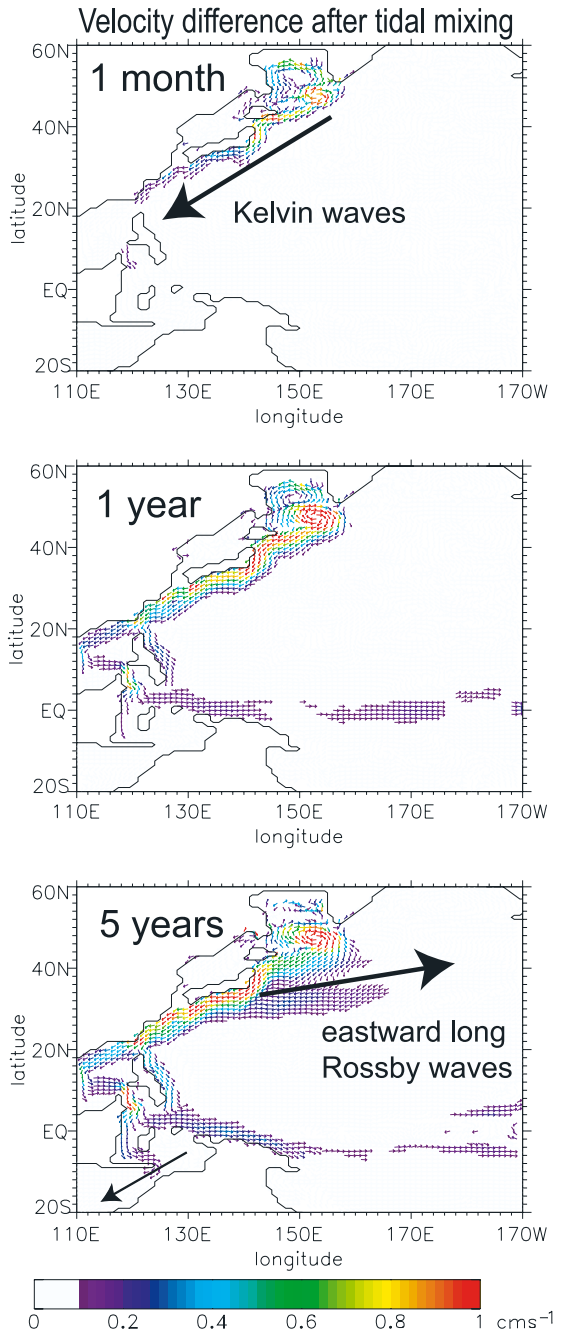

Figure 8. Initial evolution of the velocity difference between the Ctrl and Tmix cases on the 27.1σ_θ surface after addition of tidal mixing.

subtropical gyre [e.g., *Liu*, 1999; *Kubokawa and Nagakura*, 2002].

[39] Note that in the Tmix case, the thickening and deepening strengthen the Oyashio Current, which is the southward, western boundary current in the subarctic gyre flowing along the Kuril Islands. This strengthening occurs predominantly in the intermediate layer and in spring (Figure 7). Such a seasonal variation in the intermediate layer thickness and current velocity is a prominent feature of the observed Oyashio Current [e.g., *Kono and Kawasaki*, 1997b, 1997c]. The strengthened Oyashio crosses over the climatological zero-Sverdrup transport line into the subtropical gyre, as shown by *Nakamura et al.* [2006]. This feature is also consistent with observations [e.g., *Yasuda et al.*, 2001]. These results suggest the importance of tidal mixing at the Kuril Straits in driving the Oyashio Current.

4.2. Propagation of Kelvin and Rossby Modes

[40] The dynamical adjustment to the forcing at the Kuril Straits is next examined, focusing on the intermediate layer circulation. Figure 8 shows the temporal evolution of the difference in velocity between the Ctrl and Tmix cases on the 27.1 σ_θ isopycnal surface.

[41] Initially, a signal travels rapidly along the western boundary against the Kuroshio Current, and is split into two components, one propagating along the equator and the other passing through the Indonesian Archipelago and eventually reaching the Indian Ocean. This disturbance consists primarily of Kelvin waves. In fact, the mean speed of the leading front of the signal roughly agrees with that of the first mode Kelvin wave along the western boundary. The former is about 1.9 m s^{-1} since the signal travels a distance of ~5200 km from the Kuril Straits (150°E, 45°N) to the Indonesian Seas (120°E, Equator) in a month, while the latter is about 2 m s^{-1}, with the mean buoyancy frequency and the mean depth approximated as 0.003 rad s^{-1} and 2000 m, respectively.

[42] Although disturbances along the western boundary should also include other topographically trapped waves such as shelf waves, these trapped waves play a similar dynamical role in the thermohaline adjustment (i.e., topographically trapped and faster than the local currents). Thus we hereafter label all the waves responsible for this signal the "Kelvin waves" for convenience.

[43] In terms of the thermohaline adjustment, the diapycnal transport produced around the Okhotsk Sea due to both the tidally enhanced diffusion and convection converges in the intermediate layer, which therefore thickens until the convergence is compensated by horizontal flow divergence in the corresponding layer (Figure 7). Such horizontal flow divergence in turn induces mass transport away from the Kuril Straits toward the equator in the intermediate layer, a manifestation of which is the strengthening of the Oyashio Current. Simultaneously, compensating transport is induced in the shallower and deeper layers. Most of the mass is transported to the other oceans in association with the spreading of the Kelvin waves shown in Figure 8, as can be anticipated from the classical thermohaline adjustment theory of the abyssal layer [e.g., *Kawase*, 1987; *Goodman*, 2001].

[44] Interestingly, there is another signal that slowly extends eastward, moving along the boundary of the subtropical and subarctic gyres (i.e., along the flow circulation) and decaying very slowly. This behavior is characteristic of long-Rossby waves of the second and/or higher baroclinic mode under the influence of a background flow [e.g., *Rhines*, 1986; *Schopp*, 1993; *Liu*, 1999; *Thompson and Ladd*, 2004]. Some support to this interpretation can be provided by considering the phase velocity of Rossby waves, which we consider here in an approximate form since a precise form of the phase velocity is difficult to obtain [e.g., *Stephens et al.*, 2001; *Killworth et al.*, 1997].

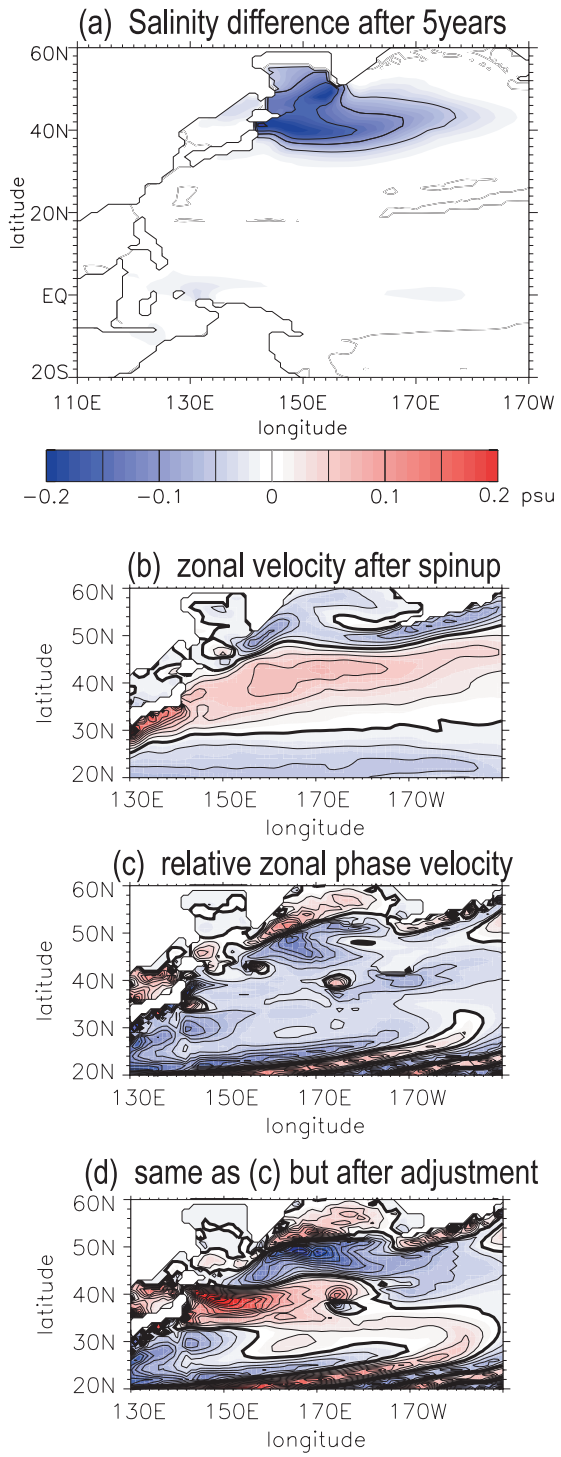

Figure 9. (a) Salinity difference distribution formed 5 years after the addition of tidal mixing, (b) zonal flow speed and (c) the relative zonal phase velocity estimated from equation (1) when tidal mixing effect is absent (an annual mean of the first year of the Ctrl run is used as the background), and (d) the same as Figure 9c but after adjusting to the tidal mixing effect (i.e., an annual mean of the last year of the Tmix run is used). Red and blue regions indicate positive and negative values, respectively. Contour interval is 0.5 cm s^{-1} in Figures 9b–9d. All of these data are calculated on the 27.1 σ_θ surface.

[45] Using quasi-geostrophic, long wave, and inviscid approximations and the assumption of a wave solution, the zonal phase velocity of small-amplitude Rossby waves, c_x, becomes

$$c_x = U - \left(\beta - \frac{\partial^2 U}{\partial y^2} - \frac{\partial}{\partial z}\left(\frac{f_0^2}{N^2}\frac{\partial U}{\partial z}\right)\right)L_n^2, \qquad (1)$$

where a background flow is approximated to be zonal and quasi-steady since the flow around the eastward extending signal is directed almost to the east. The notation is standard, U is a zonal background flow, and $L_n = N/(f_0 m)$ where m is vertical wave number [cf. *Pedlosky*, 1987; 2003]. Equation (1) shows that the propagation of Rossby waves is determined by advection (i.e., the first term) and the phase velocity relative to the background flow due to an ambient PV gradient (i.e., the second term). Hence long Rossby waves are able to move eastward where a strong eastward flow is present or the relative phase velocity is directed eastward owing to the ambient PV gradient associated with a background geostrophic flow.

[46] The equation also implies that relative phase velocity leads to a difference in speed between a passive tracer, which moves at the advective speed, and an active tracer (and/or a change in flow associated with Rossby waves), which propagates at the total phase velocity. Thus, by estimating this speed difference, we can estimate a relative phase velocity from the model results to compare it with a theoretical estimate based on equation (1).

[47] Figure 9a shows the isopycnal distribution of salinity difference, which spreads mostly owing to advection, on the 27.1 σ_θ surface as defined 5 years after the addition of tidal mixing. Over this time period, the salinity signal travels eastward by 30° $\sim$ 40° in longitude, while the corresponding velocity signal travels about 20°. Accordingly, in the zonal direction, the mean advection speed is estimated to be 1.5 $\sim$ 2 cm s^{-1}, and the mean phase speed is about 1 cm s^{-1}, yielding a relative zonal phase speed of $-0.5 \sim -1$ cm s^{-1} (i.e., westward) on average.

[48] Figures 9b and 9c show the distributions of zonal flow speed and zonal relative phase velocity, respectively, on the corresponding layer. The relative phase velocity is estimated from equation (1) with a vertical wave number of $m = n\pi/H$ where $n = 2$, so that it roughly corresponds to that of the second baroclinic mode but includes an error arising from the assumption of the WKB approximation. As the background state, the annual mean of the Ctrl case after the spinup is chosen so that the difference between the Ctrl and Tmix cases can be regarded as a perturbation. From these figures, the mean zonal advection speed and relative phase velocity are estimated to be about 1.5 cm s^{-1} and -0.5 cm s^{-1}, respectively, yielding a total phase velocity of about 1 cm s^{-1}. These values roughly agree with the above estimates based on the model results.

[49] The agreement of the theoretical estimates and model results supports the identification that the eastward moving signal is associated with long-Rossby waves. This in turn suggests that the eastward moving long Rossby waves of the second and higher modes directly affect the circulation of the interior region. It is noteworthy that after adjusting to the tidal mixing effect, relative phase velocities are also

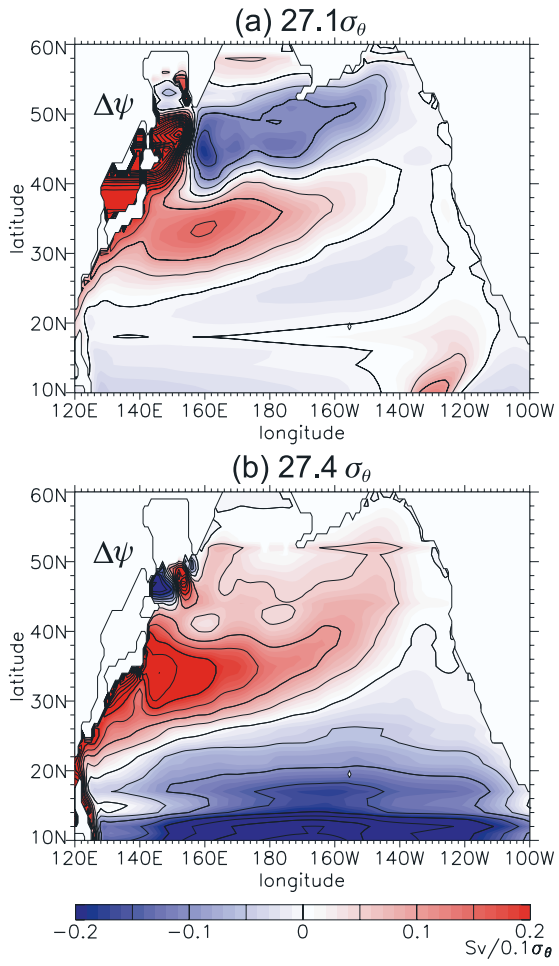

Figure 10. Difference in pseudo transport stream function between the Ctrl and Tmix cases on (a) 27.1 and (b) 27.4 σ_θ isopycnal surfaces. The pseudo-transport stream function is the same as the transport stream function when diapycnal transport is absent. Details are described in section 5.1.

directed to the east in the western part of the eastward flow region (Figure 9d). This is caused by the supply of low PV water from the Kuril Straits, which tends to direct ambient PV gradient fields there to the south and accelerates the wave speed eastward.

[50] These results suggest that both Kelvin and eastward moving long Rossby waves are required to understand the adjustment and/or circulation of the intermediate layer. The requirement of both kinds of waves is an important new aspect and is peculiar to the intermediate layer. A further discussion on this point is presented in section 7.

[51] It should be noted that the circulation paths of the freshened water supplied from the Kuril Straits (or those of the low salinity signals) are not the same as those of the Kelvin waves. This is because the Kelvin waves can travel against the Kuroshio Current, whereas the freshened water component cannot. The water thus deflects to the east into the interior region. On the contrary, the paths of eastward long Rossby waves are similar to those of the freshened water because of their wave dynamics [e.g., *Pedlosky*, 1996; *Liu*, 1999]. After deflecting eastward, the part of the freshened water that has intruded into the subtropics circulates around the gyre and then reaches the western boundary. It then joins the path of the Kelvin waves, as suggested from the distribution of salinity difference (Figure 4).

5. Effect on Circulation

[52] The adjustment through the Kelvin and eastward long Rossby waves will lead to differences in the equilibrium states of the Ctrl and Tmix cases. These are investigated here with the focus on intermediate layer circulation and meridional overturning.

5.1. Pseudo-Transport Stream Function of Intermediate Layers

[53] To investigate the difference in intermediate layer circulation between the Ctrl and Tmix cases, maps of the difference in "pseudo transport stream function" on the 27.1 and 27.4 σ_θ surfaces in the North Pacific are shown in Figure 10. The pseudo transport stream function (Ψ) on a σ_θ surface that we calculate here corresponds to that in the density layer within -0.05 to $+0.05\sigma_\theta$ from the central density. The quantity Ψ is obtained from

$$\Psi = \int_{\phi}^{\phi_e} hvR\cos\phi' d\phi',$$

where ϕ is longitude and ϕ_e is the longitude at the eastern boundary of the Pacific, h and v are thickness and meridional velocity of the density layer, respectively, and R is the Earth radius. (From this definition, a positive anomaly represents a clockwise circulation as usual.) Note that Ψ includes a divergent part if a convergence of diapycnal transport is present [e.g., *Pedlosky*, 1996]. Nevertheless, this quantity is a useful indicator of circulation in the interior region where diapycnal transport is small (although it differs from the transport stream function west of the Kuril Straits where vertical mixing is enhanced).

[54] The adjustment through Kelvin waves induces an equatorward flow anomaly along the western boundary. This feature is clearly seen on the 27.1 σ_θ surface, as a positive anomaly extending from the Kuril Straits to the equator. A similar feature is also seen on the 27.4 σ_θ surface.

[55] Since such a flow anomaly crosses the gyre boundaries, it causes an intergyre flow that leads to a more efficient transport of the freshened water from the Kuril Straits to the subtropics, and to the equatorial region. At the same time, the strengthened intergyre transport carries lower PV water from the subarctic into the subtropics and leads to a decrease in PV in the subtropical gyre. This occurs even on the 27.4 σ_θ surface, as is shown in section 3.4, since the PV values are generally smaller in the subarctic than in the subtropics.

[56] The intergyre flow also results in a latitudinal shift of the separation point of a western boundary current from the coast. In particular, the flow anomaly acts to shift the separation point of the Oyashio and Kuroshio Currents to the south by strengthening the former and weakening the latter.

[57] The eastward long Rossby wave adjustment strengthens the circulation in the northwestern part of the subtropical gyre on both isopycnal surfaces. This area roughly corresponds to the pool region estimated by *Huang and*

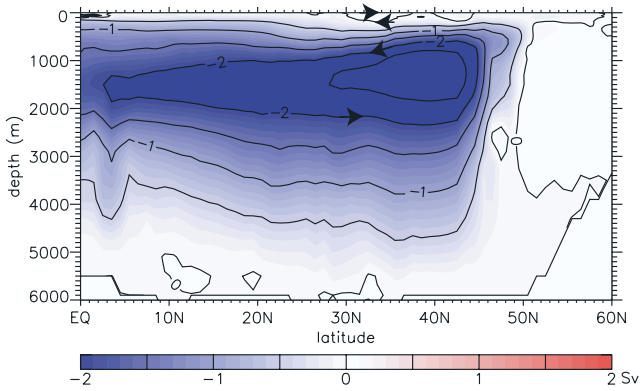

Figure 11. Difference in meridional overturning stream function in the North Pacific between the Ctrl and Tmix cases. Contour interval is 0.5 Sv.

Russell [1994]. The combination of this flow anomaly and the intergyre flow creates a water path from the Kuril Straits to the subtropical interior region, and thus leads to an enhancement of the ventilation in the subtropical intermediate layer. In addition, the circulation in the subarctic gyre is strengthened on the 27.1 σ_θ surface, but not on the 27.4 σ_θ surface, suggesting that the responses in the subarctic and subtropical gyres differ somewhat from each other. The cause of this difference is discussed in Part 2.

[58] The southwestern part of the subtropical gyre corresponding to the shadow zone is also modified, though the change is significantly weaker than that in the northwestern region. The change here is induced by the westward traveling Rossby waves originating from the Kelvin waves along the eastern boundary. Although the combination of these with the Kelvin waves plays an important role in the thermohaline adjustment theory of the abyssal layer [*Kawase*, 1987] and the adjustment to the Indonesian Throughflow [*Hirst and Godfrey*, 1993, 1994], its effect is restricted to the shadow zone in the intermediate layer. Such a restriction can be explained from the behavior of higher mode Rossby waves, as revealed in the ventilated thermocline theory [e.g., *Luyten et al.*, 1983; *Liu*, 1999]. Interestingly, the current near the equator is altered significantly on the 27.4 σ_θ surface associated with the equatorial waves, but this issue is not pursued here.

5.2. Meridional Overturning

[59] In addition to the changes in the intermediate layer flow, the shallower and the deeper layer flows are also modified in association with the forcing given at the Kuril Straits. Eventually these processes lead to the modification of meridional overturning as illustrated in Figure 11. The meridional overturning is enhanced by 3 Sv at the maximum owing to tidal mixing at the Kuril Straits, as both the shallow, clockwise overturning and deep, anticlockwise overturning are strengthened ("clockwise" and "anticlockwise" should be exchanged if the abscissa is reversed).

[60] The shallow-overturning enhancement occurs at depths shallower than about 700 m (i.e., above and within the upper intermediate layer), and is mostly visible as positive anomalies near the sea surface in the figure. Such an enhanced shallow overturning is caused mainly by the tidally enhanced convection in the Okhotsk Sea, which brings water downward.

[61] The deep-overturning enhancement occurs in the deeper region, and is somewhat emphasized in this figure compared with the shallow overturning due to the depth scale. This enhanced deep overturning is caused by the upwelling around the Kuril Straits (located around 44° to 51°N), which is in turn required to compensate the downward diffusion by tidal mixing there.

[62] These enhanced overturning circulations are associated with the strengthening of the flow toward the equator from the Kuril Straits in the intermediate layer and the flow toward the Kuril Straits in the shallower and deeper layers. Large proportions of these overturning flows leave (or enter) the North Pacific to (or from) the other basins. Consistent with this, the NPIW is observed to leak into the Indonesian Throughflow where the water properties are substantially transformed [e.g., *Lukas et al.*, 1991; *Ffield and Gordon*, 1992].

6. Sensitivity to the Tidal-Mixing Strength

[63] The comparisons of the Ctrl and Tmix cases have revealed the important effects of tidal mixing at the Kuril Straits on the water properties and circulation of the North Pacific intermediate layer. Nevertheless, the estimate of the tidal mixing strength used in the Tmix case may include significant error, as commented in section 2. This poses the

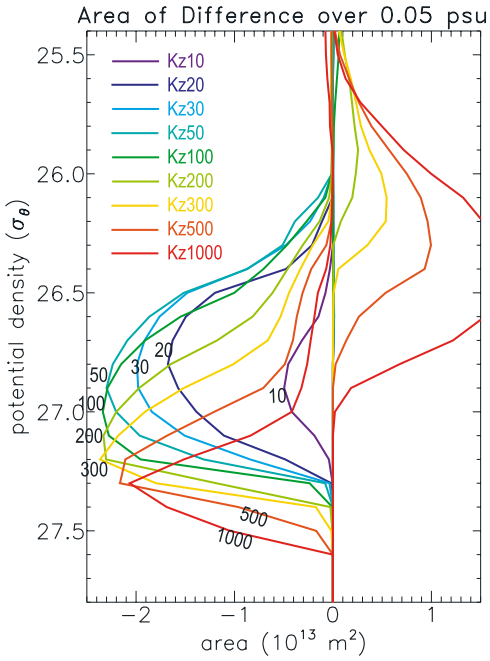

Figure 12. Area of significant freshening on isopycnal surfaces, which is plotted as a function of σ_θ for each experiment. Negative values indicate that the salinity difference is negative (i.e., freshened). Each color corresponds to one experiment (colors closer to red or blue correspond to experiments with stronger or weaker tidal mixing, respectively, as indicated by the label in cgs units). The threshold of significant difference is chosen here as 0.05 psu.

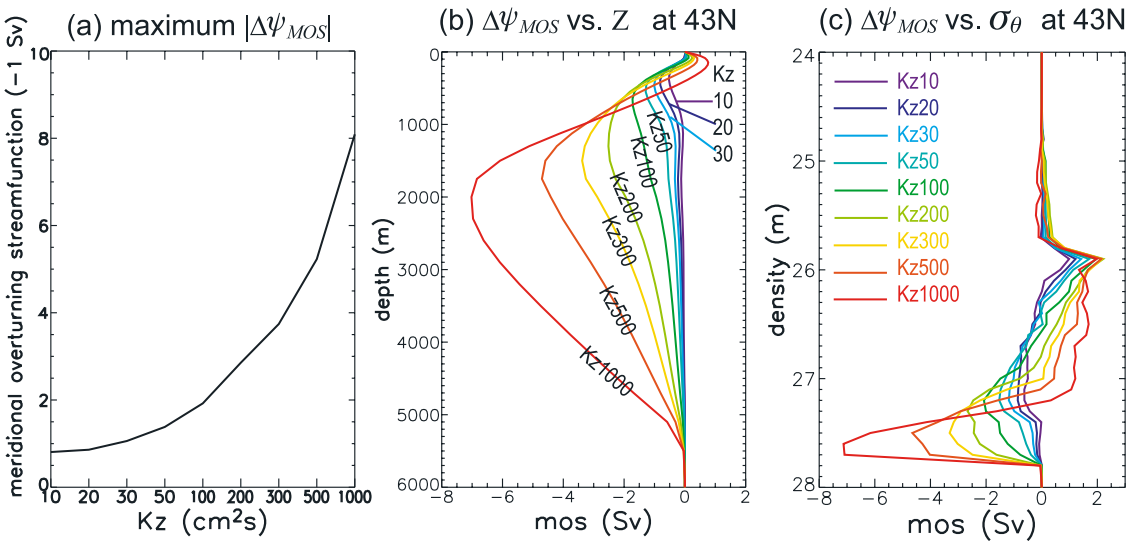

Figure 13. Changes in the meridional overturning stream function in the North Pacific from the Ctrl case ($\Delta\psi_{MOS}$) for various strength of tidal mixing. (a) Maximum differences. (b) Vertical structure of $\Delta\psi_{MOS}$ at 43°N. (c) Same as Figure 13b but σ_θ is used for the vertical coordinate.

question as to whether the effects depend on the tidal mixing strength. The sensitivity to the tidal mixing strength is therefore investigated in this section on the basis of cases Kz10 to Kz1000 shown in Table 1. The focus is on the enhancement of freshening and meridional overturning due to the addition of tidal mixing.

6.1. Freshening

[64] To compare the effect on freshening of the intermediate layer, we have calculated salinity differences from the Ctrl case on isopycnal surfaces for each experiment, and used these values to estimate the area with significant salinity difference (i.e., the lateral extent of the significantly freshened region), which is plotted as a function of σ_θ in Figure 12. A threshold value of the significant difference is chosen here as 0.05 psu. When the salinity difference becomes negative (i.e., freshened) in a particular area, this is indicated as a negative value on the figure (and vice versa).

[65] The freshening in the intermediate layer occurs in all cases, though certain quantitative differences are seen as follows. First, the maximum value of the freshened area increases with increasing tidal mixing from the Kz10 to the Kz50 cases, reaches a maximum around the Kz50 to the Kz300 cases, and then decreases with increasing tidal mixing. The first increase is simply due to increase in both the tidally enhanced convection and downward diffusion of fresher water. The latter decrease is mainly due to the fact that intense tidal mixing produces a strong tidal front along the Kuril Straits. This eventually becomes so strong that it partially blocks the subducted water in the Okhotsk Sea from inflowing into the North Pacific (not shown), and this, in turn, leads to the weakening of freshening.

[66] Secondly, the density of the maximum freshened area generally increases with increasing tidal mixing in association with the above processes. That is, deepening results from a combination of the increasing downward diffusion and the strengthening tidal front. The former spreads the freshening downward, and the latter tends to block the freshening effect of the enhanced convection in the upper intermediate layer.

[67] Last, the upper layer becomes saltier as the tidal mixing becomes strong. This is because upward diffusion of the saltier water becomes apparent as the blocking effect of the tidal front becomes significant.

6.2. Meridional Overturning

[68] Sensitivity of meridional overturning in the North Pacific is examined here with a view to defining its strength and vertical structure, on the basis of differences in the meridional overturning stream function relative to the Ctrl case. Changes in the strength of the meridional overturning are shown in terms of the maximum difference from the Ctrl case (Figure 13a). The maximum differences are all negative, indicating that these develop in the deep, anticlockwise meridional overturning cell for all the sensitivity experiments. The differences increase with increasing tidal mixing strength from −1.6 Sv to −8.2 Sv.

[69] Interestingly, the maximum difference does not linearly increase. Note that the relationship between the diffusion coefficient and the amount of upwelling (and thus meridional overturning stream function) should be linear, if we assume a major balance between downward diffusion and upward advection in the density equation (i.e., $w\rho_z \sim K_z\rho_{zz}$, as is usual on a basin scale), and assume no significant change in density stratification. Hence our result suggests that the above balance was invalid and/or that the density structure changed. In fact, the downward transport by the tidally enhanced convection is not considered in the above balance. In addition, it may alter the stratification, as implied from the PV difference seen in Figure 6.

[70] To consider the change in vertical structure, the differences in meridional overturning at 43°N, near the southern end of the Kuril Straits, are shown in Figure 13b. In general, the differences are positive in the shallower layer and negative beneath it, which is similar to the second mode structure. This structure indicates that the northward flow in the shallow and deep layers and the southward flow in

the intermediate layer are induced (i.e., southward when $\partial\Delta\psi_{MOS}/\partial z > 0$ and vice versa, where $\Delta\psi_{MOS}$ is the difference in meridional overturning stream function). Such changes in meridional circulation are associated with enhanced downwelling in the upper part where $\Delta\psi_{MOS} > 0$ and upwelling in the lower part where $\Delta\psi_{MOS} < 0$, north of 43°N. These downwelling and upwelling zones are caused by the enhanced convection in the Okhotsk Sea and vertical diffusion in the Kuril Straits, as discussed in section 4.2. Note that these features are common to all cases considered here, though the positions of both positive and negative peaks become deeper and their values increase, with increasing tidal mixing in the Kuril Straits.

[71] The positive peaks are small and are rather difficult to identify for the weak tidal mixing cases, owing to the fact that the z-coordinate is used in the definition of the meridional stream function. As a result, density increase associated with the enhanced convection is not taken into account unless it is accompanied by vertical movement, leading to underestimates of the effect of the enhanced convection. In fact, if σ_θ is used as a vertical coordinate (Figure 13c), the corresponding positive peaks become significant (1∼2 Sv) even in the weak mixing cases. This suggests the importance of the enhancement of the shallow overturning, or of the tidally enhanced convection, when viewed in the density coordinate.

[72] Overall, while the response of the North Pacific is quantitatively modified as the tidal mixing strength varies, the response is generally similar for all the cases. Accordingly, although tidal mixing strength will no doubt be estimated more precisely by future observations, the basic response and operative mechanism identified in this study will be valid within the quoted range of tidal mixing strength.

7. Summary and Discussion

[73] Tidal mixing at the Kuril Straits is likely to cause ventilation of the layers denser than 27.0 σ_θ in the North Pacific, which cannot be ventilated by direct convection. The tidal mixing in the Straits is also considered to enhance the convection in the Okhotsk Sea, which is regarded as an origin of the NPIW. In this study, we investigated the effects of tidal mixing at the Kuril Straits on the North Pacific intermediate layer by performing numerical simulation experiments with and without tidal mixing effect. The results obtained can be summarized as follows.

[74] The comparison of the above experiments suggests that tidal mixing at the Kuril Straits can enhance the ventilation in the North Pacific intermediate layer, resulting in its freshening (and an associated cooling) down to around 27.6 σ_θ. As a result, the simulated NPIW becomes fresher, deeper (and denser), and thus more realistic than the case without tidal mixing. The maximum changes in salinity and density of the NPIW core layer exceed 0.3 psu and 0.1 σ_θ, respectively.

[75] The above enhancement of ventilation can be roughly separated into three factors. (1) Tidal mixing at the Kuril Straits causes diapycnal transport through tidally enhanced convection in the Okhotsk Sea and diffusion in the Kuril Straits and thus ventilates water there, as discussed by *Nakamura et al.* [2006]. (2) The ventilated water flows into and circulates through the North Pacific intermediate layer, leading to enhanced ventilation. The enhanced ventilation (or freshening) around the NPIW core density layer is associated mainly with the tidally enhanced convection in the Okhotsk Sea, while that in the lower part of the intermediate layer is attributable to downward diffusion at the Kuril Straits. (3) The change in the outflow water in turn modifies the circulation of the intermediate layer, thus enhancing further the ventilation of the subtropical North Pacific intermediate layer.

[76] The circulation change is forced by a diapycnal transport due to both the tidally enhanced convection and diapycnal diffusion. The convection brings water from the shallower layer to the intermediate layer, while the diffusion induces entrainment from the deeper layer (and shallower layer) to the intermediate layer. Consequently, the induced diapycnal transport converges in the intermediate layer and diverges in the shallower and deeper layers, so that the intermediate layer thickens and deepens at the main exit of the Kuril Straits. The thickening induces the second and higher baroclinic mode responses, while the deepening mainly induces the first mode response. In terms of mass transport, the convergence in the intermediate layer works as a mass source and induces a flow away from the Kuril Straits, while the divergences in the shallower and deeper layers work as mass sinks capable of creating a flow toward the Kuril Straits, eventually leading to the enhancement of both the shallow and deep meridional overturning by 2−3 Sv.

[77] In the North Pacific intermediate layer, the dynamical adjustment to such mass fluxes from the Kuril Straits occurs mainly through the agency of coastal Kelvin waves and eastward moving (or advected) long Rossby waves of the second and/or higher baroclinic modes. (Equatorial Kelvin and westward Rossby waves also have a certain effect, especially in the shadow zone, but this effect is minor.) The Kelvin waves produce a flow component from the Kuril Straits to the equator along the western boundary, while the eastward long Rossby waves enhance the circulation in the pool regions, especially those in the subtropics.

[78] As a result of these flow components, water pathways are modified to enhance ventilation in the subtropical North Pacific. First, the Kelvin-wave induced flow strengthens the Oyashio Current so that it intrudes into the subtropical gyre, and thus enhances the transport of ventilated water from the subarctic to subtropical gyres. The ventilated water is then carried into the interior, circulates around the pool region and then encounters the western boundary. Some of the water leaves the subtropical North Pacific to enter the equatorial region and other basins, in response to a Kelvin-wave induced flow. Such a water pathway is similar to that of the observed NPIW.

[79] The above results illustrate the possible roles of tidal mixing at the Kuril Straits in ventilating the North Pacific intermediate layer. The results will also be useful for understanding the response of the North Pacific intermediate layer to transient fluctuations of the atmospheric and oceanic conditions around the Kuril Straits and in the Okhotsk Sea. In addition, the results have the following two important implications.

[80] 1. The results show that key elements in the dynamical adjustment of the intermediate layer to the mass flux

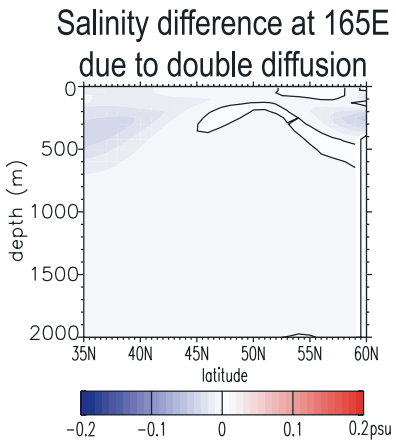

Figure 14. Same as Figure 3c, but for the difference between the Tmix case and the case without double diffusion. The setting of these two cases are the same, except for the inclusion/exclusion of a double diffusion parameterization. (The latitude range in this figure is reduced from Figure 3.)

from the Kuril Straits are coastal Kelvin and eastward long Rossby waves. This clue will facilitate development of a theoretical model of intermediate layer ventilation. Previous theories on ventilation may be categorized into ventilated thermocline theories along the lines of *Luyten et al.* [1983] and *Rhines and Young* [1982] and those of thermohaline circulation of an abyssal layer of the type developed by *Stommel and Arons* [1960] and *Kawase* [1987]. However, the former does not include the effect of mass driven Kelvin waves along the western boundary, while the latter does not represent the eastward moving long Rossby waves whose presence is established by wind driven circulation. The lack of the combined effect of these two kinds of waves may be the reason why a realistic analytical model of the ventilated intermediate layer has not been developed. Consideration of the effects of both kinds of waves will allow us to incorporate the important elements from these two major theories and therefore develop an improved theoretical model of the ventilated intermediate layer. A first step toward this unified approach is attempted in an accompanying paper (Part 2).

[81] 2. The simulated NPIW becomes fresher, deeper and denser by adding tidal mixing at the Kuril Straits. Although previous attempts to model the NPIW have succeeded in reproducing the salinity minimum, simulated NPIWs are generally saltier and shallower than observed in the ocean [e.g., *England*, 1993; *Hirst and Cai*, 1994] even when eddy permitting OGCMs are used [e.g., *Qu et al.*, 2002]. Our results suggest that one reason for this is that the effect of tidal mixing has not been taken into account either through a parameterization or through explicit reproduction. Thus attempts in the direction of the present study would lead to better numerical simulations of the ventilation of intermediate water in the North Pacific.

[82] Double diffusion and cabbeling are also considered as important mechanisms of the downward diapycnal transport required for the formation of the NPIW salinity minimum [e.g., *You et al.*, 2000; *Talley and Yun*, 2001]. However, although the effects of both double diffusion and cabbeling are included in all the above cases, the formation of the NPIW is insufficient in the case without tidal mixing. This suggests that these two effects are less important than the tidal mixing effect in the NPIW formation. In particular, when the double diffusion parameterization is excluded from the Tmix case, the resulting difference in salinity is much smaller (0.03 psu at most) and is mainly confined above the NPIW salinity minimum layer (Figure 14). This is consistent with the results of *Talley and Yun* [2001].

[83] It should be noted however that a numerical model inevitably involves some bias, which may affect a quantitative estimate. Probably the most important bias in the present case is the fact that the 26.8 σ_θ density layer is relatively shallow as compared with the observed depth. One possible cause is a small production of dichothermal water in the Bering Sea, which acts to thicken the density layer around 26.6 σ_θ [e.g., *Miura et al.*, 2002]. In addition, the simulated Kuroshio slightly overshoots to the north. Previous studies suggest that when the Kuroshio overshoots too far to the north, a relaxation boundary correction at the sea surface can cause excessive cooling due to the large temperature difference between subtropical and subarctic waters. Such cooling can result in the formation of an over deep mixed layer in winter and could affect the NPIW formation [e.g., *Kobayashi*, 1999]. Thus the separation point of the Kuroshio is shown using maps of the velocity field at 50m depth in the Ctrl case (Figure 15a). The figure indicates that the separation point of the center of the Kuroshio is located around 36°N in winter and 37°N in summer. Even the northern edge of the Kuroshio separates around 38–39°N in winter and 39–40°N in summer. (In the Tmix case, the separation point shifts southward by about one degree.) These values of the separation latitude (36–40°N) are slightly larger than those observed (around 35–37°N). Nevertheless, the simulated Kuroshio does not reach the subarctic gyre, and hence water masses in the subarctic gyre or offshore of the Kuril Islands are not directly affected. Also, the separation in our model occurs within the latitude range of the Mixed Water Region, where warm core rings arising from the Kuroshio appear very often. Thus the relaxation boundary condition is not considered to cause severe excessive cooling. In fact, previous studies suggest that an overshoot of the above extent is permissible for the investigation of the NPIW formation [e.g., *Kobayashi*, 2000]. Further, to see the sensitivity to relaxation, we have performed similar experiments but with a relaxation timescale of 30 days (i.e., the relaxation strength is doubled). The results are almost the same as the present results. As an example, the meridional section of salinity at 165E is shown in Figure 15b. Considering the above, an estimate of the relative importance of double diffusion, cabbeling, and tidal mixing in the formation of the NPIW salinity minimum in the actual ocean is beyond the scope of this paper and awaits future observational studies. Nevertheless, since the spreading of the tidal mixing effects is determined mainly by advection, Kelvin waves and eastward moving/advected long Rossby waves, which in turn are controlled mainly by the large scale flow field reproduced to reasonable accuracy here, the qualitative features of our results must remain relevant.

[84] Also, mesoscale eddies, which are present around the Kuroshio Extension in particular, are considered to induce a

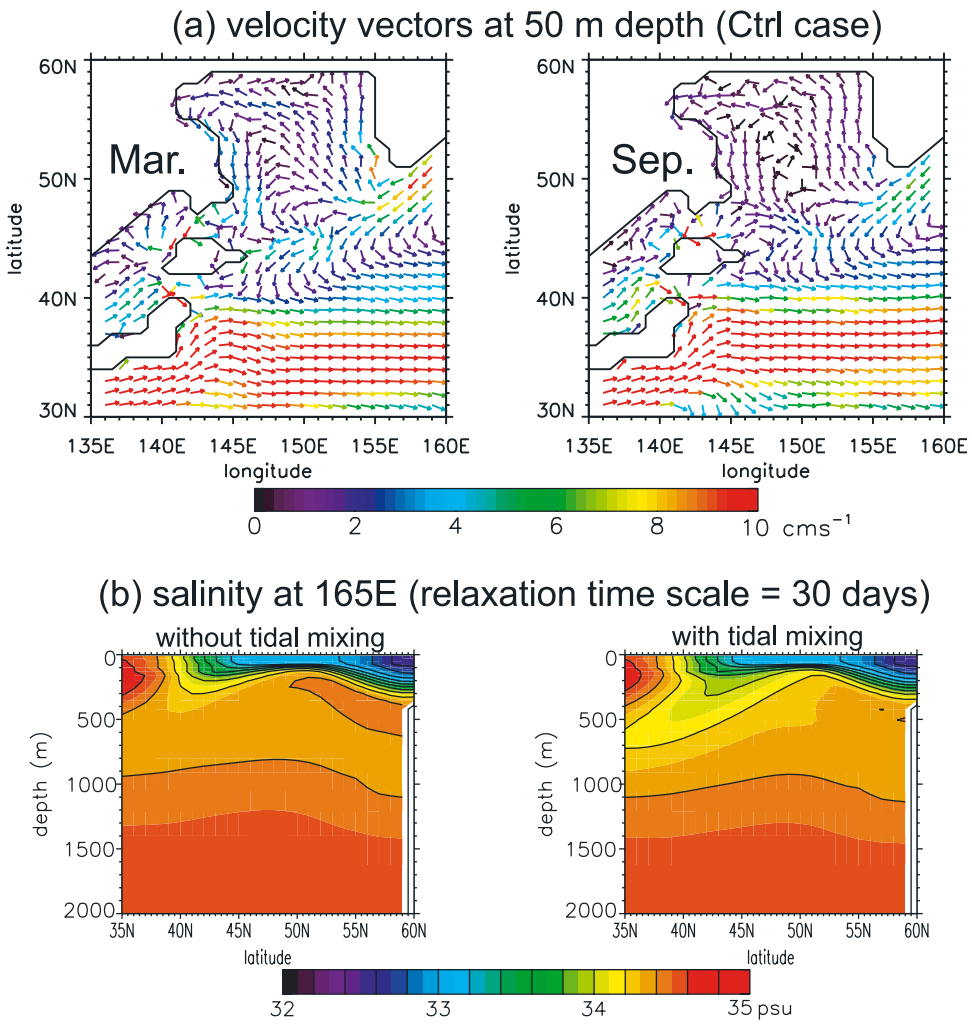

Figure 15. (a) Velocity vectors at 50 m depth of Ctrl case in (left) winter and (right) summer. (b) Meridional section of salinity at 165°E in the (left) Ctrl and (right) Tmix cases, but with a relaxation timescale of 30 days. (The latitude range is reduced from Figure 3.)

significant intergyre transport in addition to that induced through the mass-driven Kelvin waves. Such eddies are not resolved with the present model resolution, although the effect of eddies is considered using the GM90 parameterization. In addition, although the mainstream of the Oyashio separates at similar latitudes to those observed (about 40°N in winter and 42°N in summer, Figure 15a), a narrow, coastal branch of the Oyashio, which often extends further southward in winter, is not resolved. Since intergyre transport is a key element in the ventilation of the subtropical North Pacific intermediate layer, the limited resolution is also possibly the reason why the simulated NPIW in the case with tidal mixing effect is still saltier than is observed in nature. Thus an eddy resolving OGCM with tidal mixing is desirable in future for reproducing the NPIW more precisely and for a more complete understanding of intergyre transport.

[85] As discussed in section 2, the presence of a tidal flow has a number of important consequences [e.g., *Nakamura and Awaji*, 2004]. Of these, the present study focused on the effects of vertical mixing, which is considered to be important for basin-scale thermohaline circulation [e.g., *Munk and Wunsch*, 1998]. Although other processes will inevitably be involved in a complete understanding of the role of tides in North Pacific ventilation, the effect of vertical mixing must be included as it plays a central role.

[86] Although the occurrence of enhanced vertical mixing at the Kuril Straits is indicated from both observational and modeling studies [e.g., *Kawasaki and Kono*, 1994; *Gladyshev*, 1995; *Kawasaki*, 1996; *Aramaki et al.*, 2001; *Nakamura et al.*, 2000a; *Nakamura and Awaji*, 2004], there may be other regions where tidally induced vertical mixing is strong. Nevertheless, observed CFC distributions have shown that the most recently ventilated water in the lower part of the North Pacific intermediate layer (say, 27.1 to 27.6 σ_θ) lies around the Kuril Straits [*Warner et al.*, 1996; *Wong et al.*, 1998]. This observational fact implies that vertical mixing in the Kuril Straits is more effective than that in other regions around the North Pacific, at least in this density range. We thus consider that the investigation of the effects of vertical mixing around the Kuril Straits (together with the tidally enhanced convection in the Okhotsk Sea) is a useful step toward a better understanding of the ventilation of the North Pacific intermediate layer.

[87] **Acknowledgments.** We thank J. P. Matthews for reading through the manuscript. Thanks are also extended to the editor and four anonymous reviewers for their useful comments. This study is supported by the Category 7 of MEXT RR2002 Project for Sustainable Coexistence of Human, Nature and the Earth and by a Grant-in-Aid for the 21st Century COE Program (Kyoto University, G3). T. N. was partly supported by the JSPS Research Fellowships for Young Scientists. This study was done when T. N. was at Department of Geophysics, Kyoto University. Numerical calculations were done on the VPP800 at the Academic Center for Computing and Media Studies of Kyoto University.

References

Alfultis, M. A., and S. Martin (1987), Satellite passive microwave studies of the Sea of Okhotsk Sea ice cover and its relation to oceanic processes, *J. Geophys. Res.*, *92*, 13,013–13,028.

Aramaki, T., S. Watanabe, T. Kuji, and M. Wakatsuchi (2001), The Okhotsk-Pacific seawater exchange in the viewpoint of vertical profiles of radiocarbon around the Bussol' Strait, *Geophys. Res. Lett.*, *28*, 3971–3974.

Barnier, B., L. Siefridt, and P. Marchesiello (1995), Thermal forcing for a global ocean circulation model using a three-year climatology of ECMWF analyses, *J. Mar. Syst.*, *6*, 363–380.

da Silva, A. M., C. C. Young, and S. Levitus (1994), *Atlas of Surface Marine Data 1994*, vol. 1, *Algorithms and Procedures*, *NOAA Atlas NESDIS 6*, 83 pp., Natl. Oceanic and Atmos. Admin., Silver Spring, Md.

Dewar, W. K., and R. X. Huang (2001), Adjustment of the ventilated thermocline, *J. Phys. Oceanogr.*, *31*, 1676–1697.

England, M. (1993), Representing the global-scale water masses in ocean general circulation models, *J. Phys. Oceanogr.*, *23*, 1523–1552.

Fedorov, K. N. (1988), Layer thicknesses and effective diffusivities in "diffusive" thermohaline convection in the ocean, in *Small-Scale Turbulence and Mixing in the Ocean*, edited by J. C. J. Nihoul and B. M. Jamart, pp. 471–479, Elsevier, New York.

Ffield, A., and A. L. Gordon (1992), Vertical mixing in the Indonesian thermocline, *J. Phys. Oceanogr.*, *22*, 184–195.

Fine, R. A., K. A. Maillet, K. F. Sullivan, and D. Willey (2001), Circulation and ventilation flux of the Pacific Ocean, *J. Geophys. Res.*, *106*, 22,159–22,178.

Freeland, H. J., A. S. Bychkov, F. Whitney, C. Taylor, C. S. Wong, and G. I. Yurasov (1998), WOCE section P1W in the Sea of Okhotsk: 1. Oceanographic data description, *J. Geophys. Res.*, *103*, 15,613–15,623.

Gent, P. R., and J. C. McWilliams (1990), Isopycnal mixing in ocean circulation models, *J. Phys. Oceanogr.*, *20*, 150–155.

Gladyshev, S. V. (1995), Fronts in the Kuril Island region, *Oceanology, Engl. Transl.*, *34*, 452–459.

Gladyshev, S., S. Martin, S. Riser, and A. Figurkin (2000), Dense water production on the northern Okhotsk shelves: Comparison of ship-based spring-summer observations for 1996 and 1997 with satellite observations, *J. Geophys. Res.*, *105*, 26,281–26,299.

Goodman, P. J. (2001), Thermohaline adjustment and advection in an OGCM, *J. Phys. Oceanogr.*, *31*, 1477–1497.

Hasumi, H., and N. Suginohara (1999), Sensitivity of a global ocean general circulation model to tracer advection schemes, *J. Phys. Oceanogr.*, *29*, 2730–2740.

Hibiya, T., M. Ogasawara, and Y. Niwa (1998), A numerical study of the fortnightly modulation of basin-ocean water exchange across a tidal mixing zone, *J. Phys. Oceanogr.*, *28*, 1224–1235.

Hibler, W. D. (1979), A dynamic thermodynamic sea ice model, *J. Phys. Oceanogr.*, *9*, 815–845.

Hirst, A. C., and W. Cai (1994), Sensitivity of a world ocean GCM to changes in subsurface mixing parameterization, *J. Phys. Oceanogr.*, *24*, 1256–1279.

Hirst, A. C., and J. S. Godfrey (1993), The role of Indonesian Throughflow in a global ocean GCM, *J. Phys. Oceanogr.*, *23*, 1057–1086.

Hirst, A. C., and J. S. Godfrey (1994), The response to a sudden change in Indonesian Throughflow in a global ocean GCM, *J. Phys. Oceanogr.*, *24*, 1895–1910.

Huang, R. X., and S. Russell (1994), Ventilation of the subtropical North Pacific, *J. Phys. Oceanogr.*, *24*, 2589–2605.

Ikeda, M. (1989a), A coupled ice-ocean mixed layer model of the marginal ice zone to wind forcing, *J. Geophys. Res.*, *94*, 9699–9709.

Ikeda, M. (1989b), Snow cover detected by diurnal warming of sea ice/snow surface off Labrador in NOAA imagery, *IEEE Trans. Geosci. Remote Sens.*, *27*, 552–560.

Ikeda, M., T. Yao, and G. Symonds (1988), Simulated fluctuation in annual Labrador Sea-ice cover, *Atmos. Ocean*, *26*, 16–39.

Ishizaki, H., and T. Motoi (1999), Revaluation of the Takano-Oonisihi Scheme for momentum advection on bottom relief in ocean models, *J. Atmos. Oceanic Technol.*, *16*, 1994–2010.

Kawasaki, Y. (1996), The origin of the North Pacific Intermediate Water—From the observations in the Okhotsk Sea (in Japanese), *Kaiyo Mon.*, *28*, 545–552.

Kawasaki, Y., and T. Kono (1994), Distribution and transport of subarctic waters around the middle of Kuril Islands (in Japanese with English abstract and figure captions), *Sea Sky*, *70*, 71–84.

Kawase, M. (1987), Establishment of deep ocean circulation driven by deep-water production, *J. Phys. Oceanogr.*, *17*, 2294–2317.

Killworth, P. D., D. B. Chelton, and R. A. DeSzoeke (1997), The speed of observed and theoretical long extratropical planetary waves, *J. Phys. Oceanogr.*, *27*, 1946–1966.

Kitani, K. (1973), An oceanographic study of the Okhotsk Sea, particularly in regard to cold waters, *Bull. Far Seas Fish. Res. Lab.*, *9*, 45–77.

Kobayashi, T. (1999), Study of the formation of North Pacific Intermediate Water by a general circulation model and the particle-tracking method: 1. A pitfall of general circulation model studies, *J. Geophys. Res.*, *104*, 5423–5439.

Kobayashi, T. (2000), Study of the formation of North Pacific Intermediate Water by a general circulation model and the particle-tracking method: 2. Formation mechanism of salinity minimum from the view of the "critical gradient" of the Oyashio mixing ratio, *J. Geophys. Res.*, *105*, 1055–1069.

Kono, T., and Y. Kawasaki (1997a), Modification of the western subarctic water by water exchange with the Okhotsk Sea, *Deep Sea Res., Part I*, *44*, 689–711.

Kono, T., and Y. Kawasaki (1997b), Result of CTD and mooring observations southeast of Hokkaido: 1. Annual velocity and transport variations in the Oyashio, *Bull. Hokkaido Natl. Fish. Res. Inst.*, *61*, 65–82.

Kono, T., and Y. Kawasaki (1997c), Result of CTD and mooring observations southeast of Hokkaido: 2. Annual variations of water mass structure and salt flux of the Oyashio, *Bull. Hokkaido Natl. Fish. Res. Inst.*, *61*, 83–95.

Kubokawa, A., and M. Nagakura (2002), Linear planetary wave dynamics in a 2.5-layer ventilated thermocline model, *J. Mar. Res.*, *60*, 367–404.

Levitus, S., and T. P. Boyer (1994), *World Ocean Atlas 1994*, vol. 4, *Temperature*, *NOAA Atlas NESDIS 4*, 117 pp., Natl. Oceanic and Atmos. Admin., Silver Spring, Md.

Levitus, S., R. Burgett, and T. P. Boyer (1994), *World Ocean Atlas 1994*, vol. 3, *Salinity*, *NOAA Atlas NESDIS 3*, 99 pp., Natl. Oceanic and Atmos. Admin., Silver Spring, Md.

Liu, Z. (1993), Thermocline forced by varying wind: Part I. Spin-up and spin-down, *J. Phys. Oceanogr.*, *23*, 2505–2522.

Liu, Z. (1999), Forced planetary wave response in a thermocline gyre, *J. Phys. Oceanogr.*, *29*, 1036–1055.

Lukas, R., E. Firing, P. Hacker, P. L. Richardson, C. A. Collins, F. Fine, and R. Gammon (1991), Observations of the Mindanao Current during the Western Equatorial Pacific Ocean Circulation Study, *J. Geophys. Res.*, *96*, 7089–7104.

Luyten, J. R., and H. M. Stommel (1986), Experiments with cross-gyre flow patterns on a beta-plane, *Deep Sea Res.*, *33*, 963–972.

Luyten, J. R., J. Pedlosky, and H. Stommel (1983), The ventilated thermocline, *J. Phys. Oceanogr.*, *13*, 292–309.

Martin, S., R. Drucker, and K. Yamashita (1998), The production of ice and dense shelf water in the Okhotsk Sea polynyas, *J. Geophys. Res.*, *103*, 27,771–27,782.

Merryfield, W. J., G. Holloway, and A. E. Gargett (1999), A global ocean model with double-diffusive mixing, *J. Phys. Oceanogr.*, *29*, 1124–1142.

Miura, T., T. Suga, and K. Hanawa (2002), Winter mixed layer and formation of dichothermal water in the Bering Sea, *J. Oceanogr.*, *58*, 815–823.

Munk, W., and C. Wunsch (1998), Abyssal recipes II: Energetics of tidal and wind mixing, *Deep Sea Res., Part I*, *45*, 1977–2010.

Nakamura, T., and T. Awaji (2001), A growth mechanism for topographic internal waves generated by an oscillatory flow, *J. Phys. Oceanogr.*, *31*, 2511–2524.

Nakamura, T., and T. Awaji (2004), Tidally induced diapycnal mixing in the Kuril Straits and the roles on water transformation and transport processes: A three-dimensional nonhydrostatic model experiment, *J. Geophys. Res.*, *109*, C09S07, doi:10.1029/2003JC001850.

Nakamura, T., T. Awaji, T. Hatayama, K. Akitomo, T. Takizawa, T. Kono, Y. Kawasaki, and M. Fukasawa (2000a), The generation of large-amplitude unsteady lee waves by subinertial K_1 tidal flow: A possible vertical mixing mechanism in the Kuril Straits, *J. Phys. Oceanogr.*, *30*, 1601–1621.

Nakamura, T., T. Awaji, T. Hatayama, K. Akitomo, and T. Takizawa (2000b), Tidal exchange through the Kuril Straits, *J. Phys. Oceanogr.*, *30*, 1622–1644.

Nakamura, T., T. Toyoda, Y. Ishikawa, and T. Awaji (2006), Enhanced ventilation in the Okhotsk Sea through tidal mixing at the Kuril Straits, *Deep Sea Res., Part I*, in press.

Noh, Y., and H. J. Kim (1999), Simulations of temperature and turbulence structure of the oceanic boundary layer with the improved near-surface process, *J. Geophys. Res.*, *104*, 15,621–15,634.
Pedlosky, J. (1987), *Geophysical Fluid Dynamics*, 2nd ed., 710 pp., Springer, New York.
Pedlosky, J. (1996), *Ocean Circulation Theory*, 453 pp., Springer, New York.
Pedlosky, J. (2003), *Waves in the Ocean and Atmosphere*, 260 pp., Springer, New York.
Qu, T., S.-P. Xie, H. Mitsudera, and A. Ishida (2002), Subduction of the North Pacific Mode Waters in a global high-resolution GCM, *J. Phys. Oceanogr.*, *32*, 746–763.
Redi, M. H. (1982), Oceanic isopycnal mixing by coordinate rotation, *J. Phys. Oceanogr.*, *12*, 1154–1158.
Rhines, P. B. (1986), Vorticity dynamics of the oceanic general circulation, *Annu. Rev. Fluid Mech.*, *18*, 433–447.
Rhines, P. B., and W. R. Young (1982), A theory of the wind-driven circulation: I. Mid-ocean gyres, *J. Mar. Res.*, *40*, suppl., 559–596.
Röske, F. (2001), An atlas of surface fluxes based on the ECMWF reanalysis—A climatological dataset of force global ocean general circulation models, *Rep. 323*, 26 pp., Max-Planck-Inst. fü Meteorol., Hamburg, Germany.
Samelson, R. M. (1998), Large-scale circulation with locally enhanced vertical mixing, *J. Phys. Oceanogr.*, *28*, 712–726.
Sarmiento, J. L., N. Gruber, M. A. Brzezinski, and J. P. Dunne (2004), High-latitude controls of thermocline nutrients and low latitude biological productivity, *Nature*, *427*, 56–60.
Schiller, A., J. S. Godfrey, P. C. McIntosh, G. Meyers, and S. E. Wijffels (1998), Seasonal near-surface dynamics and thermodynamics of the Indian Ocean and Indonesian Throughflow in a global ocean general circulation model, *J. Phys. Oceanogr.*, *28*, 2288–2312.
Schmitt, R. W. (1981), Form of the temperature-salinity relationship in the central water: Evidence for double-diffusive mixing, *J. Phys. Oceanogr.*, *11*, 1015–1026.
Schopp, R. (1993), Multiple equilibria for cross-gyre flow between subpolar and subtropical gyres, *J. Phys. Oceanogr.*, *23*, 1754–1766.
Sirven, J., and C. Frankignoul (2000), Variability of the thermocline due to a sudden change in the Ekman pumping, *J. Phys. Oceanogr.*, *30*, 1776–1789.
Stephens, M., Z. Liu, and H. Yang (2001), Evolution of subduction planetary waves with application to North Pacific Decadal thermocline variability, *J. Phys. Oceanogr.*, *31*, 1733–1746.
Stommel, H., and A. B. Arons (1960), On the abyssal circulation of the world ocean: II. An idealized model of the circulation pattern and amplitude in oceanic basins, *Deep Sea Res.*, *6*, 217–233.
Sverdrup, H., M. Johnson, and R. Fleming (1942), *The Oceans*, 1087 pp., Prentice-Hall, Upper Saddle River, N. J.
Talley, L. D. (1991), An Okhotsk Sea water anomaly: Implications for ventilation in the North Pacific, *Deep Sea Res.*, *38*, suppl., S171–S190.
Talley, L. D. (1993), Distribution and formation of North Pacific Intermediate Water, *J. Phys. Oceanogr.*, *23*, 517–537.
Talley, L. D., and J.-Y. Yun (2001), The role of cabbeling and double diffusion in setting the density of the North Pacific Intermediate Water salinity minimum, *J. Phys. Oceanogr.*, *31*, 1538–1549.
Talley, L. D., Y. Nagata, M. Fujimura, T. Kono, D. Inagake, M. Hirai, and K. Okuda (1995), North Pacific Intermediate Water in the Kuroshio/Oyashio mixed water region, *J. Phys. Oceanogr.*, *25*, 475–501.
Thompson, L., and C. Ladd (2004), The response of the North Pacific Ocean to decadal variability in atmospheric forcing: Wind versus buoyancy forcing, *J. Phys. Oceanogr.*, *34*, 1373–1389.
Toyoda, T., T. Awaji, Y. Ishikawa, and T. Nakamura (2004), Preconditioning of winter mixed layer in the formation of North Pacific eastern subtropical mode water, *Geophys. Res. Lett.*, *31*, L17206, doi:10.1029/2004GL020677.
Uda, M. (1963), Oceanography of the subarctic Pacific Ocean, *J. Fish. Res. Board Can.*, *20*, 119–179.
Ueno, H., and I. Yasuda (2000), Distribution and formation of the mesothermal structure (temperature inversions) in the North Pacific subarctic region, *J. Geophys. Res.*, *105*, 16,885–16,897.
Van Scoy, K., D. Olson, and R. Fine (1991), Ventilation of the North Pacific Intermediate Water: The role of Alaskan Gyre, *J. Geophys. Res.*, *96*, 16,801–16,810.
Warner, M. J., J. L. Bullister, D. P. Wisegraver, R. H. Gammon, and R. F. Weiss (1996), Basin-wide distributions of chlorofluorocarbons CFC-11 and CFC-12 in the North Pacific, *J. Geophys. Res.*, *101*, 20,525–20,542.
Watanabe, T., and M. Wakatsuchi (1998), Formation of 26.8 σ_θ water in the Kuril Basin of the Sea of Okhotsk as a possible origin of North Pacific Intermediate Water, *J. Geophys. Res.*, *103*, 2849–2865.
Watanabe, Y. W., K. Harada, and K. Ishikawa (1994), Chlorofluorocarbons in the central North Pacific and southward spreading time of North Pacific intermediate water, *J. Geophys. Res.*, *99*, 25,195–25,213.
Weaver, A. J., and T. M. C. Hughes (1996), On the incompatibility of ocean and atmosphere models and the need for flux adjustments, *Clim. Dyn.*, *12*, 141–170.
Wong, C. S., R. J. Matear, H. J. Freeland, F. A. Whitney, and A. S. Bychkov (1998), WOCE line P1W in the Sea of Okhotsk: 2. CFCs and the formation rate of intermediate water, *J. Geophys. Res.*, *103*, 15,625–15,642.
Yamanaka, G., Y. Kitamura, and M. Endoh (1998a), Formation of North Pacific Intermediate Water in Meteorological Research Institute ocean general circulation model: 1. Subgrid-scale mixing and marginal sea fresh water, *J. Geophys. Res.*, *103*, 30,885–30,903.
Yamanaka, G., Y. Kitamura, and M. Endoh (1998b), Formation of North Pacific Intermediate Water in Meteorological Research Institute ocean general circulation model: 2. Transient tracer experiments, *J. Geophys. Res.*, *103*, 30,905–30,921.
Yamanaka, Y., and E. Tajika (1996), The role of the vertical fluxes of particulate organic matter and calcite in the oceanic carbon cycle: Studies using biogeochemical general circulation model, *Global Biogeochem. Cycles*, *10*, 361–382.
Yasuda, I. (1997), The origin of the North Pacific intermediate water, *J. Geophys. Res.*, *102*, 893–910.
Yasuda, I., K. Okuda, and Y. Shimizu (1996), Distribution and formation of North Pacific Intermediate Water in the Kuroshio-Oyashio interfrontal zone, *J. Phys. Oceanogr.*, *26*, 448–465.
Yasuda, I., Y. Hiroe, K. Komatsu, K. Kawasaki, T. M. Joyce, F. Bahr, and Y. Kawasaki (2001), Hydrographic structure and transport of the Oyashio south of Hokkaido and the formation of North Pacific Intermediate Water, *J. Geophys. Res.*, *106*, 6931–6942.
Yasuoka, T. (1968), Hydrography in the Okhotsk Sea: 2, *Oceanogr. Mag.*, *20*, 55–63.
You, Y., N. Suginohara, M. Fukasawa, I. Yasuda, I. Kaneko, H. Yoritaka, and M. Kawamiya (2000), Roles of the Okhotsk Sea and Gulf of Alaska in forming the North Pacific Intermediate Water, *J. Geophys. Res.*, *105*, 3253–3280.

T. Awaji and T. Toyoda, Frontier Research Center for Global Change, JAMSTEC, Yokohama, 236-0001, Japan.

Y. Ishikawa, Department of Geophysics, Kyoto University, Kyoto, 606-8502, Japan.

T. Nakamura, Institute of Low Temperature Science, Hokkaido University, Sapporo, 060-0819, Japan. (nakamura@lowtem.hokudai.ac.jp)